COMPARING EUROPEAN SEISMIC HAZARD MODELS

REPORT 2024:1013

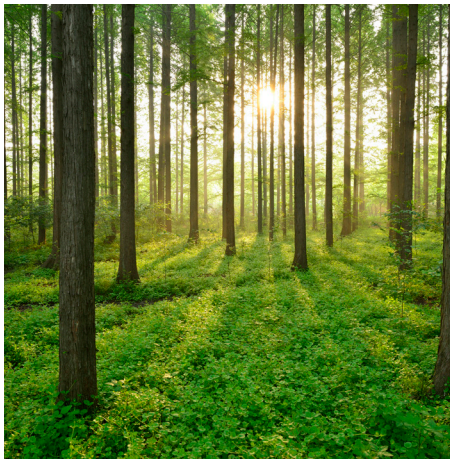

NUCLEAR POWER – OUTLOOK AND TECHNOLOGY DEVELOPMENT

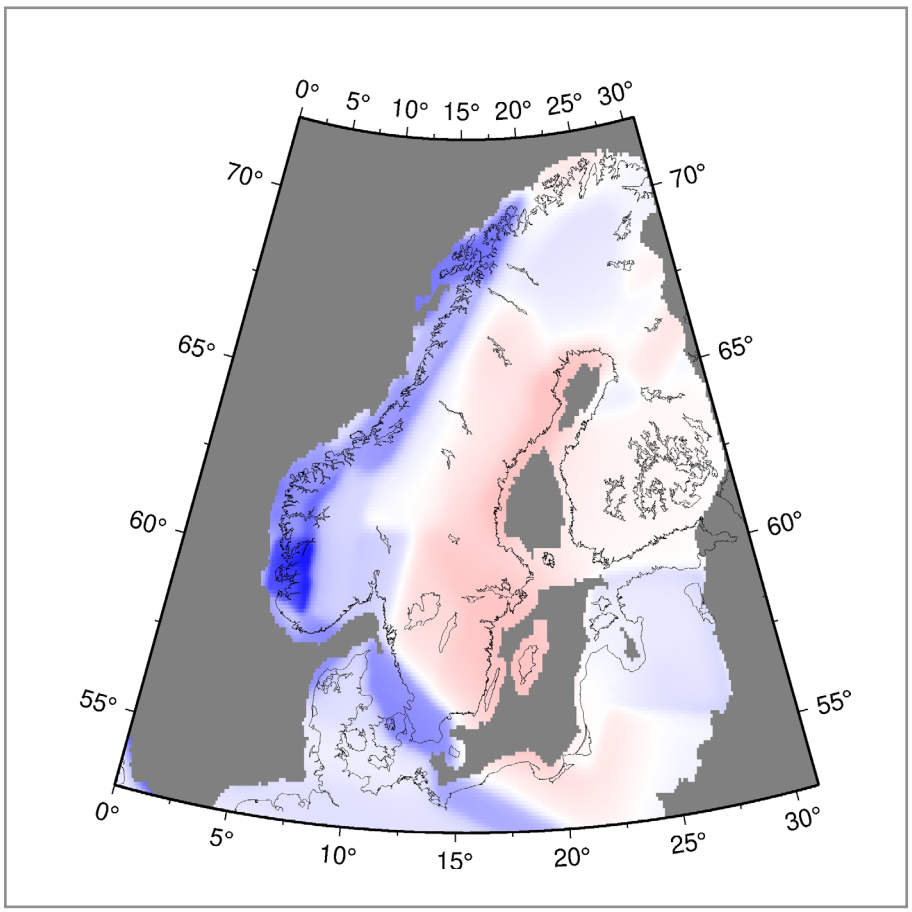

Energiforsk

Comparing European Seismic Hazard Models

ESHM20 versus ESHM13 at nuclear power plant sites in Sweden and Finland

BJÖRN LUND, UPPSALA UNIVERSITY
PÄIVI MÄNTYNIEMI, HELSINKI UNIVERSITY
AMIR SADEGHI-BAGHERABADI, HELSINKI UNIVERSITY
ANNAKAISA KORJA, HELSINKI UNIVERSITY
JAN LUNDWALL, VATTENFALL

ISBN 978-91-89919-13-6 | © Energiforsk May 2024

Energiforsk AB | Phone: 08-677 25 30 | E-mail: kontakt@energiforsk.se | www.energiforsk.se

Foreword

The Energiforsk Nuclear Portfolio aims to support long-term operation and safety in the Nordic nuclear power plants. Part of this is to follow the developments of aspects affecting safety, maintenance and development in the nuclear field.

In this study, an analysis of the differences in results between the European Seismic Hazard Model 2013 and the new, updated version European Seismic Hazard Model 2020, has been performed. Even though the ESH models are not intended for site-specific hazard analysis, they are important to understand since they form a background to international and national definitions and guidelines.

The study was carried out by Björn Lund, Uppsala University; Päivi Mäntyniemi, Amir Sadeghi-Bagherabadi and Annakaisa Korja, Helsinki University and Jan Lundwall, Vattenfall. The study was performed within the Energiforsk Nuclear Portfolio, which is financed by Vattenfall, Uniper, Fortum, TVO, Skellefteå Kraft and Karlstads Energi.

Summary

The European Seismic Hazard Model 2013 has been updated to the 2020 version ESHM20. There are systematic differences for Fennoscandia between the two versions, where western Norway, southwestern Sweden and Denmark see a decrease in hazard while the hazard has increased in most of Sweden and Finland. In this report, the origin and significance of these differences are investigated, with a special emphasis on the sites of nuclear power plants in Sweden and Finland.

The European seismic hazard model 2020 (ESHM20) supersedes the 2013 version (ESHM13) while following the same principle of state-of-the art procedures homogeneously applied for the entire pan-European region, without country-borders issues. ESHM20 includes updated datasets (earthquake catalogues, active faults, ground shaking recordings), information (tectonic and geological) and models (seismogenic sources, ground motion). For Fennoscandia, the earthquake dataset increased by eight events, but the seismic source zones were updated in the north, there was a complete change of ground motions models and the logic tree was significantly expanded. We uncovered a mistake in the update of recurrence parameters in one source zone in ESHM20 which likely has led to an overestimate of the hazard at Ringhals.

We find that the hazard, in terms of mean peak-ground-acceleration (PGA), has increased from ESHM13 to ESHM20 at the nuclear power plants (NPPs) in Olkiluoto, Forsmark, Oskarshamn and for long return periods in Loviisa. It has decreased at Ringhals and for short return periods at Loviisa. In addition, the standard deviations of the PGA distributions have increased considerably at all locations except at Ringhals, where the increase is more modest. The differences between ESHM13 and ESHM20 are likely due mostly to the complete update of ground motion models, the significantly expanded logic tree and improved methodologies and algorithms.

Assessing the significance of the differences between two hazard models is a long-standing problem in seismic hazard. We applied four different tests to the models, addressing different aspects of the model results. The test results were inconclusive in that some tests indicated robust differences while others did not. It is important to note that neither ESHM13 nor ESHM20 are intended as site-specific hazard models, they are not applicable to annual probabilities of exceedance below $2 \cdot 10^{-4}$, or return periods beyond 5000 years, and do not replace national hazard models.

ESHM20 only uses earthquakes with magnitude 3.5 or higher, which severely limits the amount of data from Fennoscandia. The expansion of the Fennoscandian seismic networks and the thriving collaboration between them has enabled the recording of tens of thousands of earthquakes in the last 25 years, mostly below magnitude 3.5. Using the smaller events makes it possible to calculate recurrence parameters based on statistically significant data sets in more area zones, thereby better accounting for spatial variations in seismicity. There are therefore possibilities to significantly improve seismic hazard models for Fennoscandia.

Keywords

Probabilistic seismic hazard analysis (PSHA), seismic hazard map, European Seismic Hazard Model 2013 (ESHM13), European Seismic Hazard Model 2020 (ESHM20), nuclear power plant, Sweden, Finland

Seismisk fara, karta över seismisk fara, Europeisk modell av seismisk fara, ESHM13, ESHM20, kärnkraftverk, Sverige, Finland

Sammanfattning

Den europeiska modellen för seismisk fara från 2013 har uppdaterats till 2020 versionen. För Fennoskandien är det systematiska skillnader mellan de två versionerna, där västra Norge, sydvästra Sverige och Danmark fått minskad fara medan faran har ökat i stora delar av Sverige och Finland. I den här rapporten studerar vi orsaker till och signifikansen av dessa skillnader, med fokus på platserna där de svenska och finska kärnkraftverken är belägna.

Den europeiska modellen för seismisk fara version 2020 (ESHM20) ersätter 2013 versionen (ESHM13) enligt samma princip om bästa möjliga metodik homogent tillämpad över hela den europeiska regionen, utan påverkan av landsgränser. ESHM20 inkluderar uppdaterade data (jordskalvskataloger, aktiva förkastningar, markrörelser), information (tektonisk och geologisk) samt modeller (seismiska källzoner, markrörelse). I det Fennoskandiska området ökade jordskalvsdatat med endast åtta skalv men de seismiska källzonerna uppdaterades i norr, helt nya markrörelsemodeller tillämpades och det logiska trädet utökades signifikant. Vi upptäckte ett misstag i hur återkomstparametrarna i den källzon där Ringhals är belägen hade uppdaterats, vilket inneburit att den seismiska faran där överskattats något i den slutgiltiga modellen.

Den seismiska faran, i termer av maximal markacceleration (PGA), har ökat från ESHM13 till ESHM20 för kärnkraftverken i Olkiluoto, Forsmark och Oskarshamn samt för långa återkomsttider i Loviisa, medan den har minskat i Ringhals och för korta återkomsttider i Loviisa. Dessutom har standard-avvikelserna i PGA-fördelningarna ökat stort för alla platser utom för Ringhals, där ökningen är lägre. Skillnaderna mellan ESHM13 och ESHM20 beror sannolikt till största delen på de ändrade markrörelsemodellerna, det utökade logiska trädet och förbättringar i metoder och algoritmer.

Att utvärdera signifikansen av skillnader mellan två seismiska faromodeller är ett klassiskt problem. Vi har tillämpat fyra olika tester på de två modellerna, dessa testar olika aspekter på skillnaderna mellan dem. Testresultaten är inte samstämmiga, några tester indikerar att skillnaderna är robusta medan andra hävdar motsatsen. Det är viktigt att ta i beaktande att varken ESHM13 eller ESHM20 är menade som platsspecifika faromodeller, de är inte menade för årliga sannolikheter mindre än $2 \cdot 10^{-4}$, eller återkomstperioder på mer än 5000 år, och de ersätter inte nationella modeller av seismiska fara.

I ESHM20 används bara jordskalv med magnitud 3,5 eller större, vilket gör att den innehåller mycket lite data från Fennoskandien. Utökningen av de Fennoskandiska seismiska näten och det goda samarbetet mellan de nordiska seismiska näten har gjort att vi registrerat tiotusentals jordskalv under de senaste 25 åren, de allra flesta med mindre magnitud än 3,5. Genom att använda de mindre skalven för beräkningar av återkomstparametrar ökas den statistiska signifikansen, vi kan bättre ta hänsyn till den rumsliga variationen och därmed signifikant förbättra modeller av seismisk fara för Fennoskandien.

List of content

1. Introduction

Long-term challenges of planning, seismic design and construction ultimately determine the safety of structures against external hazards such as earthquakes. In this report, earthquake-related hazards are exclusively associated with the vibratory ground motions triggered by natural earthquakes. Secondary earthquake effects, such as tsunamis and landslides, or other types of ground failure, are not considered. Possible increase of natural seismicity rates with earthquakes induced or triggered by the alteration of the stress field due to human activity (mining, filling of large water reservoirs, enhanced geothermal systems, etc.) is not considered either.

The ground-motion hazard should preferably be evaluated by using probabilistic and deterministic methods of seismic hazard analysis (IAEA 2016). Deterministic methods typically specify a particular earthquake or level of ground shaking to be considered, by determining single-valued parameters such as earthquake size (magnitude), location (hypocenter) or peak ground acceleration (PGA). An advantage is that additional characteristics of the ground motion can be modeled, such as critical pulses or non-stationarity of motion (McGuire 1995). The deterministic approach does not usually specify how likely the future scenario might be, only that it is rare but considered possible. Uncertainties are incorporated by using a conservative process at each step of the analysis (IAEA 2016), but they typically deal only with the ground shaking uncertainties.

Seismic design is based on an assessment of future seismicity rates which are unknown to us but which are assessed assuming that earthquake occurrences of the recent past are key to seismicity in the near future. The formalized stochastic procedure is known as probabilistic seismic hazard assessment (or analysis; PSHA), a methodology used to estimate the probability that a threshold value of a selected ground-motion parameter will be exceeded at a target site or region during a given period, as outlined by Cornell (1968), following largely from the collaboration between Allin Cornell, Luis Esteva and others (McGuire 2008). Today it is the de facto standard procedure for seismic hazard analysis worldwide (e.g., Budnitz et al. 1997; Solomos et al. 2008; Hanks et al. 2009; USNRC 2012). PSHA requires an assessment of earthquake sources and occurrence, ground-motion prediction equation (GMPE), an appropriate probability level, and a choice of shaking intensity levels. The primary outcomes of site-specific PSHAs are seismic hazard curves and uniform hazard spectra (UHS), while the results of PSHAs over multiple sites can be presented as seismic hazard maps. PSHA is the first, necessary measure toward seismic risk analysis and the implementation of risk reduction strategies. The standard parameter presented is the horizontal peak ground acceleration (PGA) for a return period of 475 years, which is equivalent to the 10% exceedance (90% non-exceedance) probability of the given shaking intensity in 50 years. Time spans of 30 to 50 years are typically an engineering demand for building code purposes.

In PSHA, statements about future seismicity are expressed in terms of probability, a mathematical concept that allows predictions to be made in the face of uncertainty. PSHA combines multiple component models and their uncertainty to produce a hazard result. Two types of uncertainty are typically associated with PSHA: The aleatory (alternatively random or stochastic) variability is inherent in natural phenomena, and epistemic uncertainty refers to the lack of knowledge concerning the validity of the models and the numerical values of their parameters (e.g., Budnitz et al. 1997). Epistemic uncertainty can, in concept, be reduced by collecting new observations and developing modeling, but the collected data are often not sufficiently abundant for the rejection of any hypotheses about future seismicity. Esteva (1969) introduced aleatory variability to GMPEs.

Although equivalent and in widespread use, expressing probability levels as return periods has been criticized by Gerstenberger et al. (2020) as misleading, since return periods imply regularity of occurrence. They state that regularity is not correct, neither in the case of the time-memoryless Poisson process nor any time-dependent seismicity model. There is therefore a move towards expressing the probabilities in terms of the annual probability of exceedance (e.g., Danciu et al. 2024). Return periods of 50, 475, 975, 2475 and 5000 years correspond to annual probabilities of exceedance 0.02, 0.0021, 0.001, 0.000404 and 0.0002, respectively.

The logic-tree framework was introduced to PSHA by Kulkarni et al. (1984). The various assumptions of the input data can also be treated quantitatively using Monte Carlo analysis (McGuire 1993), but it is currently standard practice to integrate the designed scenarios of earthquake occurrence into the PSHA in a logic-tree structure. Logic trees serve as tools that capture and quantify the epistemic uncertainty of the seismic source zone and GMPE models (e.g., Bommer et al. 2005). Epistemic uncertainty is expressed in a set of branch weights, by which an expert (group) assigns degree-of-belief values to the applicability of the corresponding branch models. If the logic tree covered all the mutually exclusive and completely exhaustive (MECE) and appropriately weighted future earthquake scenarios, the result could be interpreted as the true hazard distribution (Bommer and Scherbaum 2008). However, the MECE conditions are not always fulfilled; for example, input models can be based on shared data, such as different GMPEs relying on the same ground-motion recordings. More detailed discussion about uncertainties in PSHA models can be found for example in Gerstenberger et al. (2020).

National seismic hazard models are typically developed to generate seismic design values for the national building codes for residential, commercial and industrial buildings. The national seismic hazard models are updated as new data and knowledge become available. A useful national map must estimate hazard with a consistent methodology across the country. The national mapping efforts cannot be replaced by larger-scale work; however, large-scale projects have acted as

important spurs for the development and harmonization of PSHA practices. For example, preparation of the first global seismic hazard map in the 1990s (Giardini and Basham 1993) significantly increased the standardization of PSHA practices and cross-border cooperation worldwide.

In Europe, the global seismic hazard map of the 1990s was succeeded by uniform seismic hazard modeling for the Mediterranean region that is seismically the most active part of the continent. The project Seismotectonics and Seismic Hazard Assessment of the Mediterranean Basin (SESAME; Jiménez et al. 2001) aimed at homogeneous seismic hazard computations. In particular, it focused on redesign of seismic source zones across border areas to avoid ambiguities and design of new source zones in areas where no previous zoning was available. As many national seismic hazard models were gradually updated but were often based on different, non-harmonized procedures, a new project was planned to overcome the challenges of hazard mapping in border areas. The project Seismic Hazard Harmonization in Europe (SHARE) was funded for the period 2009-2013. Its primary objective was to provide a reference hazard model for Europe and Türkiye. It also aimed at providing the necessary input for the seismic provisions of the European building code Eurocode 8 (EC8; CEN 2004). The SHARE project resulted in the 2013 European Seismic Hazard Model (ESHM13; Woessner et al. 2015). The ESHM13 is one of the two pan-European seismic hazard models we explore in this report. The second model is the 2020 European Seismic Hazard Model (ESHM20; Danciu et al. 2021, 2024).

The ESHM13 was updated to ESHM20 in the framework of Seismology and Earthquake Engineering Research Infrastructure Alliance for Europe (SERA) project in 2017–2020, a large community composed of 28 work packages. The work benefitted from close collaboration with the Global Earthquake Model Foundation (GEM). In particular, the GEM team maintains and develops the OpenQuake platform for the hazard calculation (Pagani et al. 2014). The update continued the principles laid in the SHARE project: Data compiled homogeneously across country borders and full scientific integration of all the disciplines involved. The differences between ESHM13 and ESHM20 are perused in more detail in Section 2. Besides the updated seismic hazard map, the SERA project produced the first European seismic risk map (ESRM20; Crowley et al. 2021).

The update of the European seismic hazard model coincided with the preparation of the second-generation EC8. Strong interaction including several technical discussions between the EC8 and the ESHM20 core teams took place. In October 2021, the ESHM20 seismic hazard maps for Europe for a return period of 475 years were included as an Informative Annex in the second-generation EC8. The ESHM20 maps were considered as “an acceptable representation of the seismic hazard in Europe for the return period of 475 years.”

Sweden and Finland are low-seismicity countries that are currently not part of EC8 and have no official mandate for a national seismic hazard map. Site-specific PSHAs are conducted for critical infrastructure, such as Nuclear Power Plants (NPP). The pan-European seismic hazard maps are useful references here, and the high level of sophistication in the applied methodology may stimulate the national hazard work. Whenever new PSHA results become available, it is natural – in practice automatic – to compare them to the previous ones for the same region. The question that then arises is how to quantify the observed differences. Construction requires stability in the design levels, and an increase in seismic hazard level ultimately affects the cost of seismic design.

In this report, we explore and compare the PSHA results of the ESHM13 and ESHM20 models at five NPP sites in Sweden and Finland (Forsmark, Oskarshamn, Ringhals; Loviisa, Olkiluoto; Figure 1). We largely rely on Douglas et al. (2023) who conducted an extensive literature search on the comparison of PSHA results. Their search included conference proceedings that are not always easily accessible. Douglas et al. (2023) have since withdrawn their submitted manuscript, but the search results nevertheless remain usable to us. Their search yielded just four criteria to quantifying the differences, despite the prevalence and need of comparison between hazard values for the same site. These criteria are given and used for the five NPP sites under consideration in Section 3.

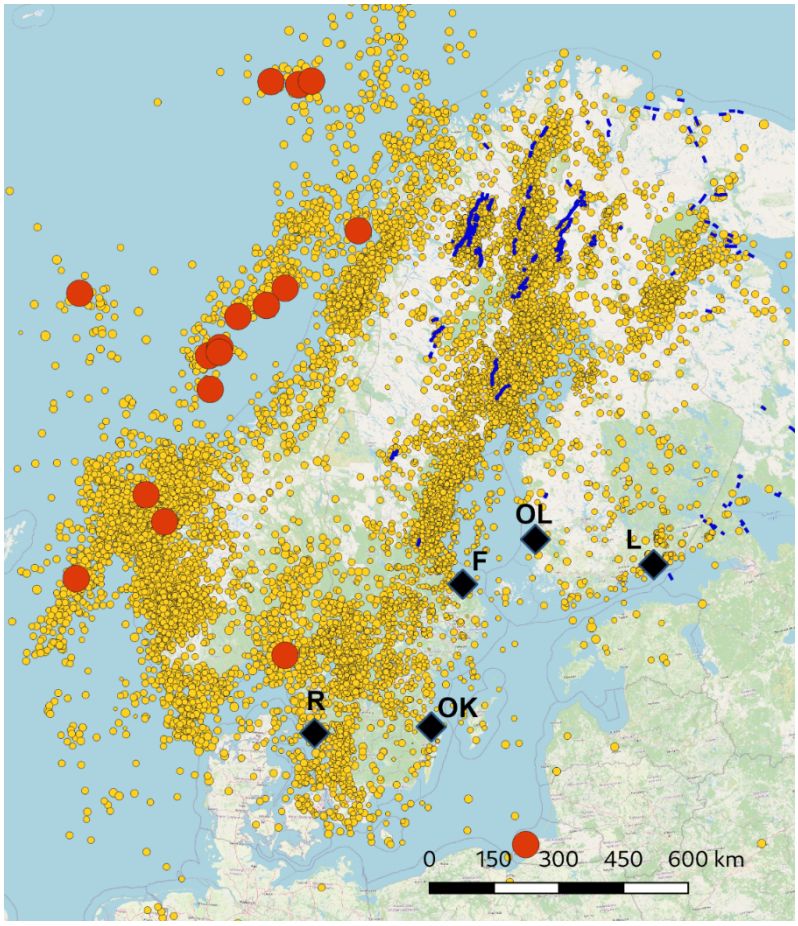

Figure 1. ***Seismicity of northern Europe between 1875 and 2022 (orange and red circles). The symbol size is relative to magnitude, which vary between -1 and 6, earthquakes with magnitude M ≥ 5 with red circles. The blue lines denote post-glacial faults. The black diamonds show the five nuclear power plant sites of interest: Forsmark (F), Oskarshamn (OK), Ringhals (R) in Sweden, Loviisa (L) and Olkiluoto (OL) in Finland.***

This report is structured as follows: Section 2 presents general information about the European models ESHM13 and ESHM20. Section 3 compares ESHM13 and ESHM20 in more detail with a focus on Fennoscandia. In particular, it includes a comparison between ESHM13 and ESHM20 at the five NPP sites of interest. Section 4 discusses how uncertainties in the hazard components are being investigated in Fennoscandia, Section 5 describes the significant increase in earthquake data in Fennoscandia since the early 2000s, and Section 6 reviews seismic hazard work in Fennoscandia since the 2010s. Section 7 is a discussion, and Section 8 has conclusions.

2. The European Seismic Hazard Models

The pan-European seismic hazard projects have produced extensive sets of results. The ESHM13 and ESHM20 maps, specifying a 10% probability of exceedance of PGA for an exposure time of 50 years, corresponding to a return period of 475 years, constitute the reference hazard maps. In addition, results have been computed for different levels of ground motion and different exposure times. The ESHM13 work produced in total over five hundred maps that depicted the probabilities of exceedance in the range 1–50% in 50 years and a number of periods of ground acceleration from PGA (usually 0.02 s or 0.01 s) to 10 s. Hazard curves, UHS and hazard disaggregation schemes were computed for over 120,000 sites spaced at 10 km across Europe and Türkiye (Woessner et al. 2015).

The ESHM20 updated and extended the ESHM13 following the same principles with state-of-the art procedures homogeneously applied for the pan-European region and Türkiye, and with data compilation and methods harmonized across country borders. The ESHM20 outputs include hazard maps for PGA and spectral acceleration with 5% damping at predominant periods in the range of 0.05 s to 5 s and five mean periods (50, 475, 975, 2500 and 5000 years). Hazard curves were calculated at each computational site for the mean, median and the quantiles 5^{th}, 16^{th}, 84^{th} and 95^{th} for all intensity measure types. UHS were estimated at each computational site depicting the mean, median and four quantiles (5^{th}, 16^{th}, 84^{th}, 95^{th}) and five mean return periods (50, 475, 975, 2500 and 5000 years). Disaggregation schemes were calculated for all sites (Danciu et al. 2021, 2024).

An update of the ESHM13 was warranted since there was an elevated level of knowledge from many countries having updated their national hazard models (e.g., Germany, Romania, Spain, Switzerland, Türkiye) and a significant increase in earthquake data and information in Europe. The primary datasets relevant to PSHA are earthquake catalogs for the pre-instrumental and instrumental eras, a database on active faults, and ground shaking records. Tectonic and geological information is included. Improved models on seismogenic sources and ground shaking attenuation were available.

The pre-instrumental catalog of the ESHM20 covered the period 1000–1899 and aimed at a balance between cross-border harmonization and regional and national knowledge. The macroseismic data points (MDP) were derived from the European PreInstrumental earthquake CAtalogue (EPICA; Rovida and Antonucci 2021; https://doi.org/10.13127/epica.1.1). Homogeneous parametrization was applied to the MDPs retaining the strategy of ESHM13. The final pre-instrumental catalog included 5703 earthquakes with macroseismic intensity ≥ 5 or moment magnitude (M_w) ≥ 4.0. ESHM13 had 4963 earthquakes in the same period.

The instrumental catalog covered the years 1900–2014. The main increase of data followed from adding the years from 2007 to 2014 to the ESHM13 catalog and from lowering the minimum magnitude from the M_w 4.0 used in the ESHM13 to M_w 3.5 uniformly throughout Europe. There were in total 61,127 earthquakes, where 54,791 were shallow (depth < 40 km), in the updated instrumental catalog. ESHM13 had a total of 30,012 earthquakes of which 25,666 where shallow (Danciu et al. 2021). Most of the data increase obviously came from the high-seismicity Mediterranean region and Türkiye.

An example of data increase is also the pan-European Engineering Strong Motion (ESM) flatfile (Lanzano et al. 2019). It contains more than 20,000 strong motion records and their associated metadata. The records are represented by peak ground motion values, response spectral accelerations and Fourier spectra. The amount of data exceeds the dataset available for the ESHM13 by almost an order of magnitude. However, most of the increase is in the magnitude range $4 \leq Mw \leq 5$. The rarity of earthquakes at the higher end of the magnitude-frequency relationship means that there can be large epistemic uncertainties regarding maximum credible magnitudes throughout Europe.

The compilation of seismogenic faults relied mainly on publicly available datasets and additionally contributed datasets over larger regions or locally targeted areas of interest. The subduction zones in the eastern Mediterranean and the intermediate-depth seismicity of Vrancea, Romania required specific modeling. Besides active faults, areal seismic sources were delineated throughout Europe.

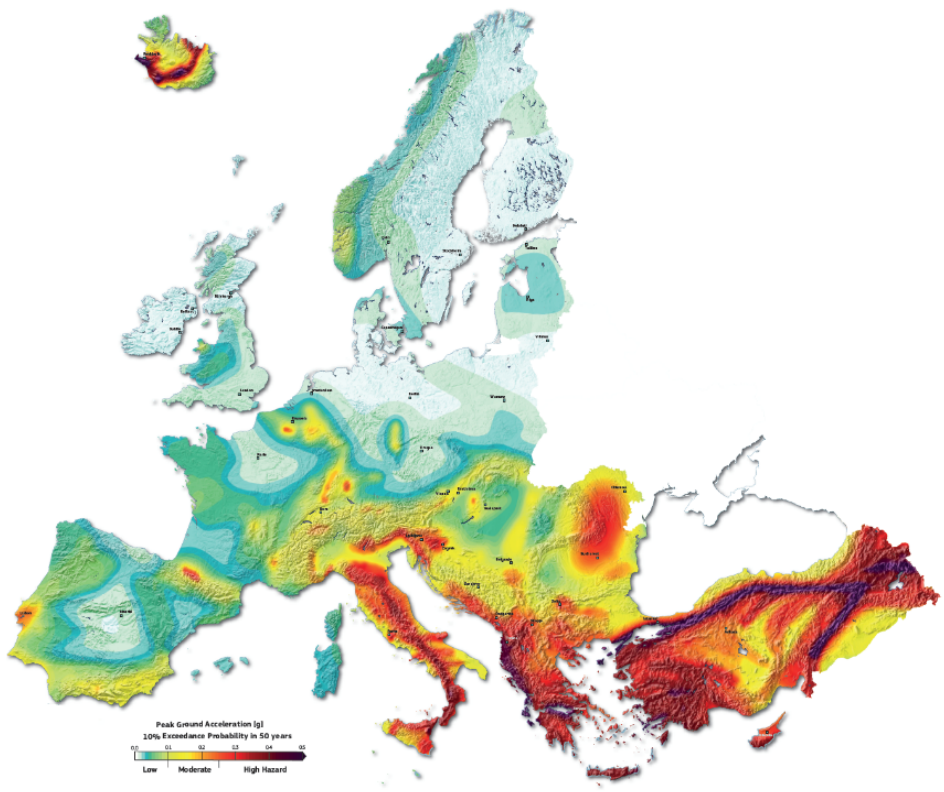

Figure 2. ***The European Seismic Hazard Map 2013 (ESHM13) displaying peak ground acceleration values in units of g for the 475-yr return period. Note: the darkest red-purple colour corresponds to 0.5 g. Source:http://hazard.efehr.org/export/sites/efehr/.galleries/dwl_europe2013/SHARE_ESHM_PGA475y.png***

Modeling ground motion is a major challenge for PSHA, so the development of the ground motion model (GMM) logic tree for a given region should aim to characterize the expected ground motion due to earthquakes, the aleatory variability, epistemic uncertainty and differences between regions. Delavaud et al. (2012) constructed a logic tree for ground-motion prediction in Europe for the ESHM13. They used an expert- and data-driven procedure for the selection and weighting of GMPEs such that the logic tree captured epistemic uncertainty in the GMMs for six different tectonic regimes in Europe. The ESHM20 GMMs were adapted from the framework proposed by Douglas (2018). The main new features were new models for shallow crust by Kotha et al. (2020) used as the default backbone in the shallow crustal GMM by Weatherill et al. (2020). Interesting for Fennoscandia, Weatherill and Cotton (2020) developed a new non-parametric model for northeastern Europe (Sweden, Finland and the Baltic countries) since the default GMM cannot be assumed to be valid in these regions. The new model was derived using the suite of Next Generation Attenuation (NGA) East models by Goulet et al. (2018) who investigated eastern North America. Subduction and deep seismicity were calibrated by Weatherill et al. (2023a).

Figures 2 and 3 show the reference hazard maps of ESHM13 and ESHM20, respectively. They, as all other results from the respective projects, are based on a time-independent hazard model, i.e., it is assumed that earthquakes occur with a

constant average frequency, but independently of each other (e.g., Cornell 1968). An approximate comparison of Figures 2 and 3 draws on the spatial distribution of seismic hazard and the relative hazard between different regions. The high seismicity of the eastern Mediterranean basin, the Northern and Eastern Anatolian fault zones, Italy, southern Spain and Portugal, and Iceland follow the active plate boundaries; the intermediate-depth seismicity in Vrancea, Romania; and the low seismicity of Fennoscandia, where western Norway exhibits the highest seismicity, are features expected to be displayed in any scientifically sound hazard map. A comparison suggests that the ESHM13 gives higher hazard levels than the ESHM20 in many high-seismicity parts of Europe and Türkiye. In the low-seismicity United Kingdom, the spatial distribution of hazard appears to be rather similar in both maps, whereas in the Swedish and Finnish territories the spatial distribution has higher variability.

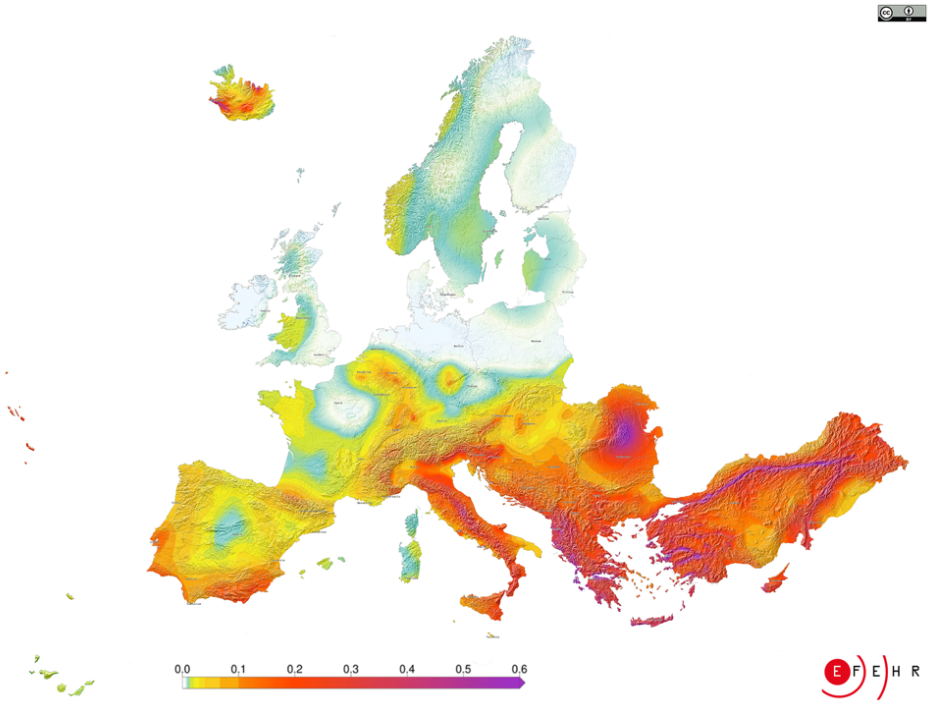

Figure 3. ***The European Seismic Hazard Map 2020 (ESHM20) displaying peak ground acceleration values in units of g for the 475-yr return period. Note: The purple colour corresponds to 0.6 g. Source: http://www.efehr.org/earthquake-hazard/hazard-map/***

An approximate comparison attributes differences in the spatial distribution of seismic hazard between two maps to the seismic source models used and the differences in the level of hazard to data increase and ground-motion models. Given the complexity of the input data preparation and hazard calculation, it is difficult to precisely pinpoint the specific causes of the differences. Techniques such as drawing hazard contours may also cause an apparent increase in the hazard level at an individual site: the new hazard value can move the site to the next level of contouring, even though the actual difference between the two hazard values is small (Douglas et al. 2014).

Danciu et al. (2021) quantified the differences in the hazard values of the ESHM13 and ESHM20 maps numerically (Figure 4). The difference map shows that the ESHM20 gives lower hazard levels in many parts of Europe, and an increased hazard in Vrancea in Romania, in parts of Spain and Greece, and western Türkiye. Western Norway and southwestern Sweden has lower hazard, while the hazard in much of the rest of Sweden appears slightly increased. The difference between the two models in Fennoscandia is discussed in more detail in Section 3.

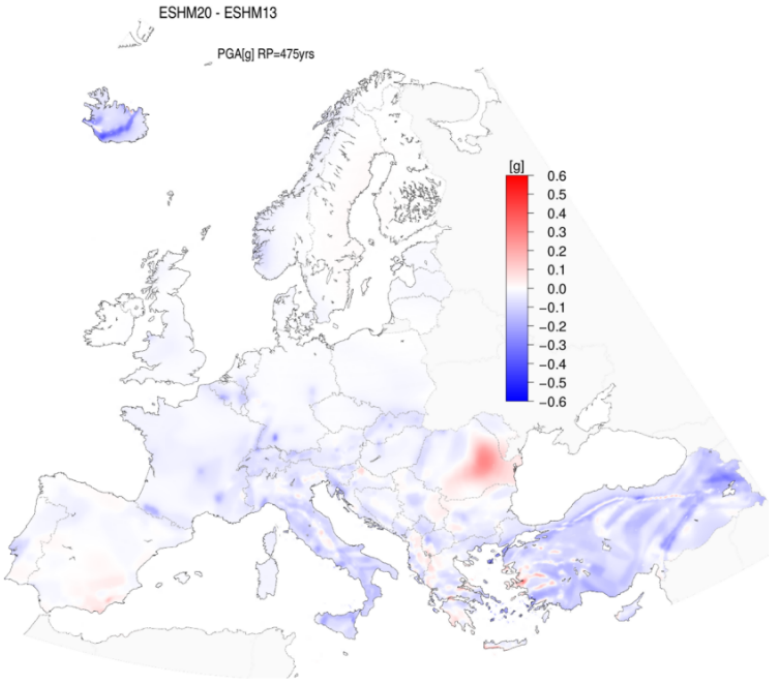

Figure 4. ***A map of spatial variability of the PGA [g] difference on mean values of the ESHM20 versus ESHM13 for a return period of 475 years. Red colour indicates an increase of PGA values when compared with the ESHM13 estimates, and the blue colour indicates a decrease. Source: Danciu et al. (2021).***

PSHAs generate new information that serves many users with different needs. Given the complexity of the models and computations, as well as the role of expert judgments in the process, there is a strong demand for transparency. It does not only apply to the input data and models used, but also to the entire process and results. The ESHM13 and ESHM20 work devoted significant effort to transparently document and openly store all data, results and methods. They are made available through the European Facilities for Earthquake Hazard and Risk (EFEHR) platform (www.efehr.org). The EFEHR is a non-profit network of organizations and community resources aimed at advancing seismic hazard and risk analysis in Europe.

3. Comparing ESHM20 to ESHM13 in Fennoscandia

This section discusses the differences between ESHM20 and ESHM13 in more detail, with a focus on Fennoscandia. Information comes from Woessner et al. (2015) for ESHM13, Danciu et al. (2021, 2024) for ESHM20 and data available from the EFEHR portal. The description here is by no means exhaustive as both models are constructed with a large number of parameters and parameter choices. It is intended to give an overview of the main components in the models. In subsection 3.3.5 numerical comparisons are made between the two models at the five NPP sites in Sweden and Finland, with the aim of better quantifying the significance of any differences.

3.1. SEISMICITY, SOURCE ZONES AND RECURRENCE ESTIMATES

Although the ESHM20 earthquake catalog updated the ESHM13 catalog with events from 2007 to 2014 and lowered the magnitude threshold from Mw 4.0 to Mw 3.5, the update only increased the onshore and near-shore Fennoscandian part of the catalog by 8 events, from 362 in ESHM13 to 370 in ESHM20. From ESHM13 to ESHM20, 14 events were removed after identifying them as non-earthquakes and 22 events were added, some from the 2007–2014 period, some newly identified from historical times (Figure 5). The two very active source zones on the southwest coast of Norway, bordering Bergen, contain no change in the number of events, even though that is not clear from Figure 5. The data shown in Figure 5 are the unified and declustered earthquake catalogs from the two models. ESHM20 retains the magnitude homogenization scheme from ESHM13 (Grünthal and Wahlström 2012) with only minor exceptions. Four of the Fennoscandian events have revised magnitudes that differ more than ±0.1, of these three historical events have lower and one 1988 North Sea event has higher magnitude.

In order to calculate the parameters needed to estimate seismic activity and recurrence rates, i.e. the lowest magnitude above which all earthquakes are detected (the magnitude of completeness, Mc), the frequency-magnitude distribution parameters (a- and b-values) and the largest possible earthquake magnitude (the maximum magnitude, Mmax), ESHM13 and ESHM20 both use two different approaches in the Fennoscandia region. One is based on area source zones, where the parameters are constant within the zone, and the other is referred to as smoothed seismicity, where a smoothing kernel is passed geographically through the data and the parameters calculated at each grid point. The results from the two approaches define two branches in the final logic tree (Section 3.3). The algorithms used for the calculations, both for area sources and the smoothed seismicity, have changed from ESHM13 [double truncated Gutenberg-Richter (Weichert 1980); Bayesian penalized maximum likelihood (Johnston et al. 1994; Coppersmith et al. 2012); smoothing (Hiemer et al. 2014)] to ESHM20 [double truncated Gutenberg-Richter (GEM 2022), Pareto tapered distribution (Kagan and

Jackson 2000), smoothing algorithm (GEM 2022)]. These methodologies are implemented in the OpenQuake engine (Pagani et al. 2014; GEM 2022), a software package for seismic hazard and risk calculations used in both ESHM13 and ESHM20. They are also discussed in Danciu et al. (2024).

The ESHM13 seismic source zone definitions were updated in ESHM20 (Figure 5) most notably in northern Fennoscandia where new polygons were added in response both to the recently recorded post-glacial fault activity and activity in the Kuusamo region, Finland. Interestingly, that seismicity is not visible in Figure 5 (compare to Figure 1) as the event magnitudes are mostly below Mw 3.5. There is, however, a significant impact on the estimation of activity rates in the polygons as the number of events per polygon changes from ESHM13 to ESHM20.

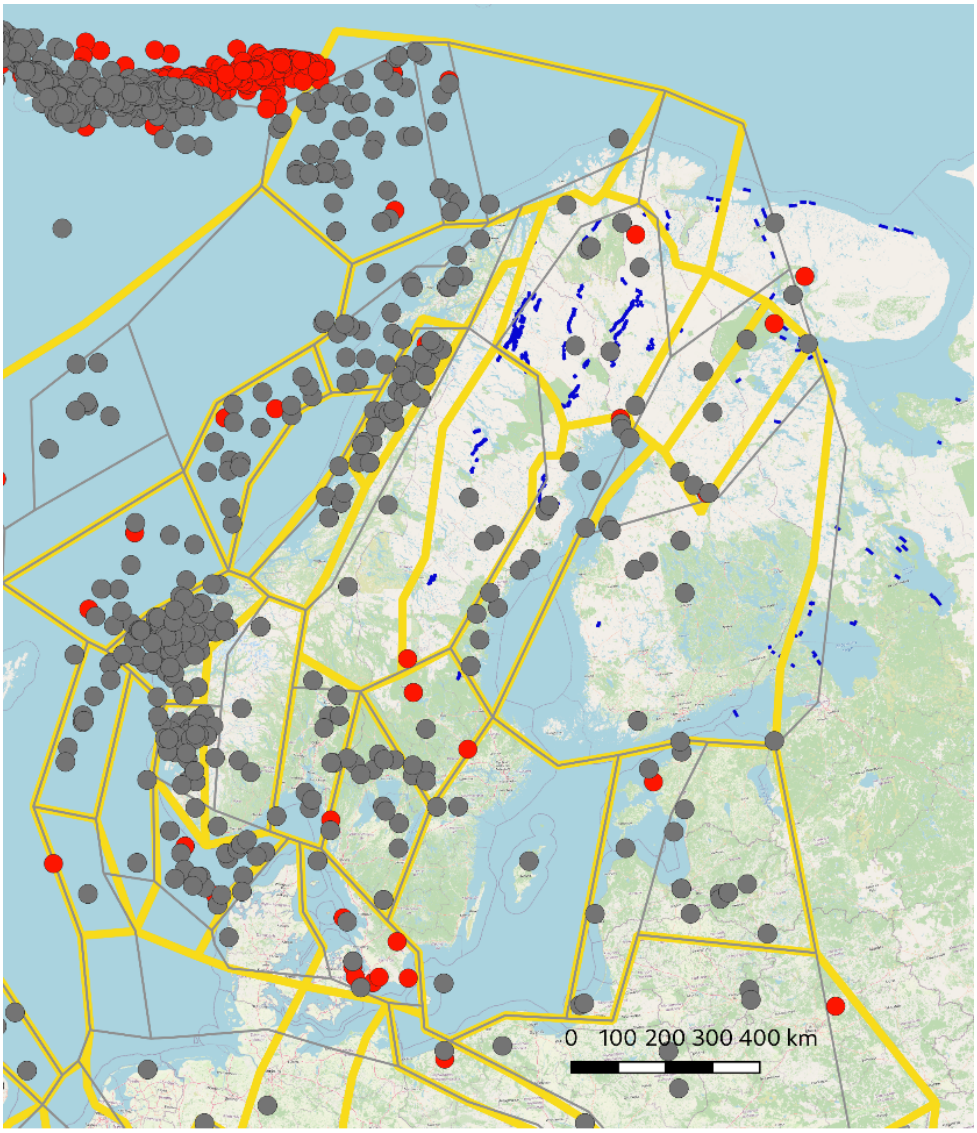

Figure 5. ***Maps showing the ESHM13 earthquakes (grey) plotted on top of the ESHM20 earthquakes (red) and the ESHM13 seismic source zones (grey) plotted on top of the ESHM20 source zones (yellow). Post-glacial faults are shown in blue. Data from https://www.efehr.org/***

As is obvious from Figure 5, many of the area zones in Fennoscandia do not contain enough events for a statistically sound assessment of the recurrence parameters, they are instead calculated in larger superzones (ESHM13) or completeness superzones and tectonic source zones (ESHM20), which are different in ESHM13 and ESHM20. For area source zones with too few events (ESHM20 requires at least 30 events above the completeness magnitude), b-values are assigned directly from the larger zones, whereas a-values are rescaled depending on the number of events in the zones. The rescaling is done based on the ten-logarithm of the ratio of the complete number of events (i.e., the number of events with magnitude larger or equal to the magnitude of completeness) in the smaller and larger zones. If there are no complete events in the smaller zone, the rescaling is done based on the logarithm of the relative area of the smaller to the larger zone. For comparison, the recurrence parameters used for the area source zones

encompassing the NPPs in Sweden and Finland are listed in Table 1 for ESHM13 and ESHM20.

In ESHM13, the a- and b-values in all three zones in Table 1 stem from the superzones. Similarly, in ESHM20 all three area source zones (Table 1 and Figure 6) have their a- and b-values inherited from superzones. The full input data for ESHM20 is available at the ESHM20 GitHub, linked to from efehr.org. The source zones are described in shape files, including the recurrence parameters for the zones and how they have been inherited from larger zones. Unfortunately, the inheritance of the recurrence parameters from larger to smaller source zones for the three zones of interest here is not consistent between the input shape files. Communication with Laurentiu Danciu in February 2024 showed that:

- The area source zones with Oskarshamn (SEAS414) and Forsmark/Olkiluoto/Loviisa (FIAS159) inherit recurrence parameters from tectonic source zone TSZ026. As that zone also has too few events, the recurrence parameters stem from completeness zone SZ31. However, the shape files for SEAS414, FIAS159 and TSZ026 erroneously point to completeness zone SZ15. SZ15 has b-value 0.91, the reference should have been to SZ31 which has b-value 1.0, and which provide the b-value inherited and used by the smaller TSZ026 and the two areas source zones. The a-values for the smaller zones are rescaled from the SZ31 a-value. Note that TSZ026 overlaps significantly with SZ31, SZ15 and SZ10, see Figure 6, and should perhaps have been defined differently.
- The shape file for the area source zone with Ringhals (SEAS409) indicates that recurrence parameters are inherited from tectonic zone TSZ007 and completeness zone SZ49. SEAS409 is located in these zones, see Figure 6, but the SEAS409 recurrence parameters have erroneously been inherited from an earlier version of zonation and does not correspond to any of the TSZ or SZ in the region. As SEAS409 does not have enough events for a separate recurrence parameter calculation it should have inherited the b-value from TSZ007, which has a b-value of 1.04. The larger completeness zone SZ49 has b-value 0.94. TSZ007 has 190 events with magnitude equal to, or larger than, the magnitude of completeness whereas SEAS409 only has 3 such events (L. Danciu, private communication, 2024). This implies that SEAS409 should have had an a-value of 2.29.

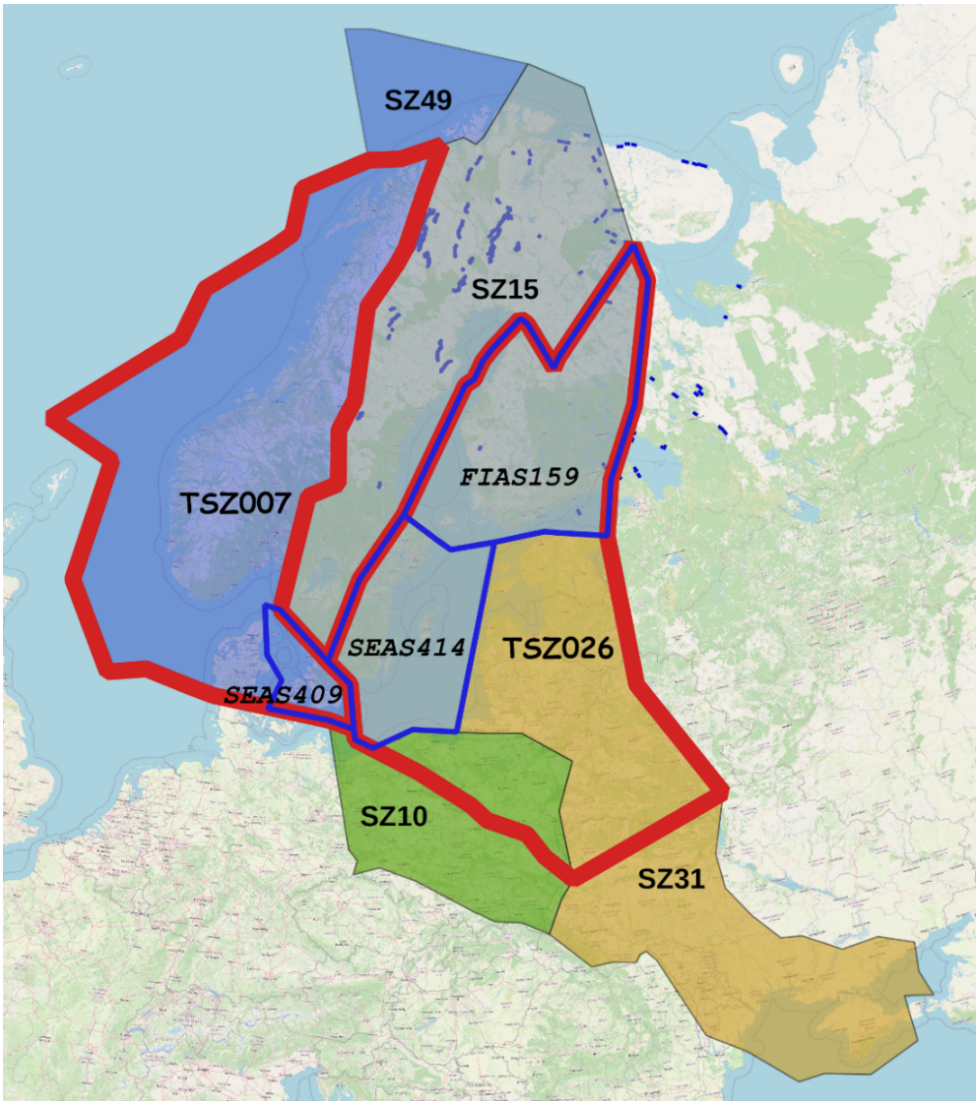

Figure 6. ***Seismic source zones used for recurrence parameter inheritance in ESHM20, see text. Colored completeness zones (SZ10: green; SZ15: grey; SZ31: yellow; SZ49: blue), tectonic source zones TSZ007 and TSZ026 shown by thick red lines along the borders, area source zones SEAS409, SEAS414 and FIAS159 shown by thinner blue lines along the borders.***

Table 1. Recurrence parameters for the area source zones in ESHM13 and ESHM20 containing the nuclear power plants (NPP) in Sweden and Finland. "Src area": area source zone designation, "N": total number of earthquakes in the zone, "a, b": parameters of the frequency-magnitude distribution, "Mmax": Maximum magnitude.

	ESHM13					ESHM20				
NPP	**Src area**	**N**	***a***	***b***	**Mmax**	**Src area**	**N**	***a***	***b***	**Mmax**
Ringhals	SEAS030	4	2.95	1.00	6.5 – 7.1	SEAS409	10	1.65 ±0.06	0.84 ±0.09	6.3 – 6.9
Oskars-hamn	SEAS978	4	2.04	1.00	6.5 – 7.1	SEAS414	3	2.51 ±0.01	1.00 ±0.01	6.3 – 6.9
Forsmark /Olkiluoto/Loviisa	FIAS032	8	2.10	1.00	6.5 – 7.1	FIAS159	9	2.33 ±0.01	1.00 ±0.01	6.3 – 6.9

Table 1 shows that the recurrence parameters estimated for the NPP zones have changed significantly, i.e. beyond the one-sigma uncertainty estimates in ESHM20 (there are no published uncertainties for ESHM13). This is related both to differing definitions of the superzone boundaries used, and thus the number of events included, for the recurrence parameter estimations and to the modernized algorithms. For the Oskarshamn and the Forsmark/Olkiluoto/Loviisa zones, the b-values are 1.0 in all instances but the a-values have increased from ESHM13 to ESHM20. An increased a-value indicates a higher activity rate, i.e. a larger number of events per unit time and therefore decreased return periods for a particular magnitude. For Oskarshamn, the increase in a-value implies that the return period for a magnitude 6.0 (M6.0) earthquake has decreased from 9120 years in ESHM13 to 3090 years in ESHM20. For Forsmark/Olkiluoto/Loviisa the corresponding decrease is from 7943 years in ESHM13 to 4677 in ESHM20.

For Ringhals there are significant changes in both the recurrence parameters. We note that due to the logarithmic scaling of the frequency-magnitude relationship, calculations of return periods are very sensitive to changes in both a- and b-values. For SEAS409, the large decrease in a-value, implying lower seismicity rates and thus fewer M6.0 events, is to a certain degree counteracted by the decrease in b-value, which acts to increase the number of large events relative to the number of small events. The parameter change for the Ringhals area implies that the estimated return period for a M6.0 earthquake has increased from 1122 years in ESHM13 to 2455 years in ESHM20. Using the a- and b-values from TSZ007 which SEAS409 in ESHM20 probably should have had, i.e. 2.29 and 1.04 as discussed above, the a-value is still significantly lower than in ESHM13 whereas the b-value is very similar. This decrease in estimated activity rate while the b-value stays approximately the same increases the return period for a M6.0 earthquake to 8913 years, much longer than in ESHM13.

The area source zone approach to recurrence parameter estimation in ESHM20 is complemented by the smooth seismicity approach, which uses the b-values from the tectonic source zones. For the Oskarshamn and Forsmark/Olkiluoto/Loviisa locations those are the same b-values as for the area source zones in Table 1. For Ringhals, the smoothed seismicity method uses a b-value of 1.04, as in tectonic zone TSZ007 (L. Danciu, private communication, 2024). a-values are rescaled smoothly in accordance with the location of seismicity in the tectonic zones.

The range of Mmax values used for cratonic regions in ESHM13 is based on a global compilation into a single distribution by Wheeler (2009, 2011). ESHM13 sets the lowest value to 6.5 and add three values with an increase of 0.2 (6.7, 6.9 and 7.1). In ESHM20, the lowest Mmax is determined by the largest observed magnitude in the magnitude superzone, which for the very large superzone where Fennoscandia is located is 6.3. Two additional values with an increase of 0.3 are used (6.6 and 6.9). The highest Mmax then corresponds statistically to a historical record of approximately 5000 years (Danciu et al. 2018). The decrease from ESHM13 to ESHM20 in the range of Mmax values used affects both the recurrence parameter estimation and the final hazard calculation, where different Mmax are included as branches in the logic tree (Section 3.3). It is therefore difficult to assess the impact of this change on the results without explicit calculations beyond the scope of this report.

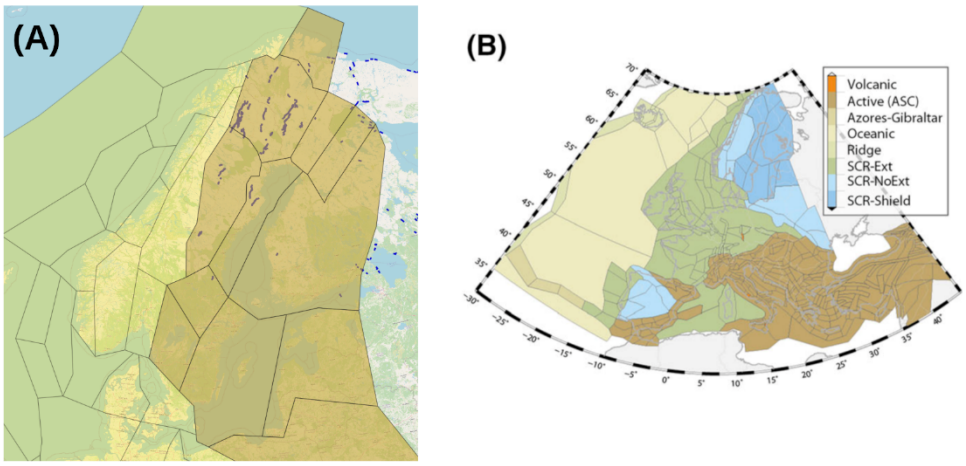

Figure 7. ***Maps showing the tectonic regionalisation of (A) ESHM20 in the region of Fennoscandia and (B) ESHM13. In (A) the dark yellow is the Shield region and the bright yellow the stable continental region. In terms of GMM, the Shield region is modelled with the cratonic GMM and the Stable continental region using the Shallow Default GMM (Danciu et al. 2021). (B) is from Woessner et al. (2015)***

3.2. GROUND MOTION MODELS

As alluded to in Section 2, the ground motion models (GMMs) were to a large extent either revised or replaced in going from ESHM13 to ESHM20. As GMMs have a decisive impact on seismic hazard assessment, these changes potentially cause significant changes in the hazard results, although the exact impact may require calibration runs to assess. For Fennoscandia, the tectonic regionalization, and thus the used GMMs, changed between the two models, with ESHM13 assigning westernmost Norway, Denmark and the Swedish west coast to "Stable Continental Region (SCR)–Extended", central Norway and the Caledonides to

"SCR–Non-extended", and most of Sweden, Finland and most of the Baltic countries to "SCR-Shield", see Figure 7. In terms of GMMs, the SCR-Extended and SCR-Non-extended regions were assigned five different GMMs with equal weight: Campbell (2003), Toro (2002, unpublished), Cauzzi and Faccioli (2008), Akkar and Bommer (2010) and Chiou and Youngs (2008). The SCR-Shield regions were only assigned Campbell (2003) and Toro (2002, unpublished) with equal weights, see also Section 3.3. Ringhals is assigned to the SCR-Extended region whereas Oskarshamn and Forsmark/Olkiluoto/Loviisa are assigned to the SCR-Shield region.

ESHM20 uses only two tectonic definitions for the Fennoscandian GMMs, "Shallow Default" for most of Norway, Denmark and the Swedish west coast, and "Craton" for most of Sweden, Finland and the Baltic countries, see Figure 7. The Shallow Default areas use the Weatherill et al. (2020) scaled backbone concept of constructing a GMM logic tree that capture epistemic uncertainties in ground motion variability for shallow crustal seismic sources in Europe. The Craton regions instead use the Weatherill and Cotton (2020) ground motion logic tree, created with a similar scaled backbone concept but utilizing data from Central and Eastern North America through the NGA-East project (Goulet et al. 2018). The Craton GMM also includes a branch of the Shallow Default model, with a weight of 0.2 based on the Fülöp et al. (2020) GMM named FennoG16, see Section 3.3. Ringhals is assigned to the Shallow Default region whereas Oskarshamn and Forsmark/Olkiluoto/Loviisa are assigned to the Craton region.

Note that both ESHM13 and ESHM20 uses a Vs30 value of 800 m/s (EC8 class A) as reference rock for all GMMs, also in the cratonic regions.

3.3. HANDLING UNCERTAINTIES: THE LOGIC TREE

Uncertainties, both epistemic and aleatory, are accounted for in probabilistic seismic hazard analysis by the use of a logic tree (e.g., Danciu et al. 2021). The logic tree may contain branches with different approaches to the same problem, such as using different seismic source models (e.g. area source, smoothed seismicity, active faults), different computational methods (e.g. for calculation of recurrence parameters) or accounting for uncertainties in parameters. Each branch has an associated weight, defined such that at each branching point the outgoing branches add up to weight 1. Defining the individual branch weights is a delicate problem which, for certain types of branching such as different computational methods or different Mmax, is commonly assigned using expert opinion or expert elicitation (e.g., Budnitz et al. 1997).

The main points of the ESHM13 logic tree are shown in Figure 8. For Fennoscandia, the Fault Source and BackGround (FSBG) source model is not used, as there are no defined active faults in Fennoscandia in ESHM13. Weights of 50-50 are used between the AS and the SEIFA (L. Danciu, private communication, 2024). Each area source zone, or each grid point in SEIFA, is associated with an a- and a b-value (no branches for a- and b-value uncertainties could be used due to computational restrictions (L. Danciu, personal communication, 2024)). The logic

tree then branches out in four different Mmax values, each of which branch out in a number of different GMMs, depending on the source zone. Hazard is calculated for all branches of the logic tree and integrated into a final hazard, or ground

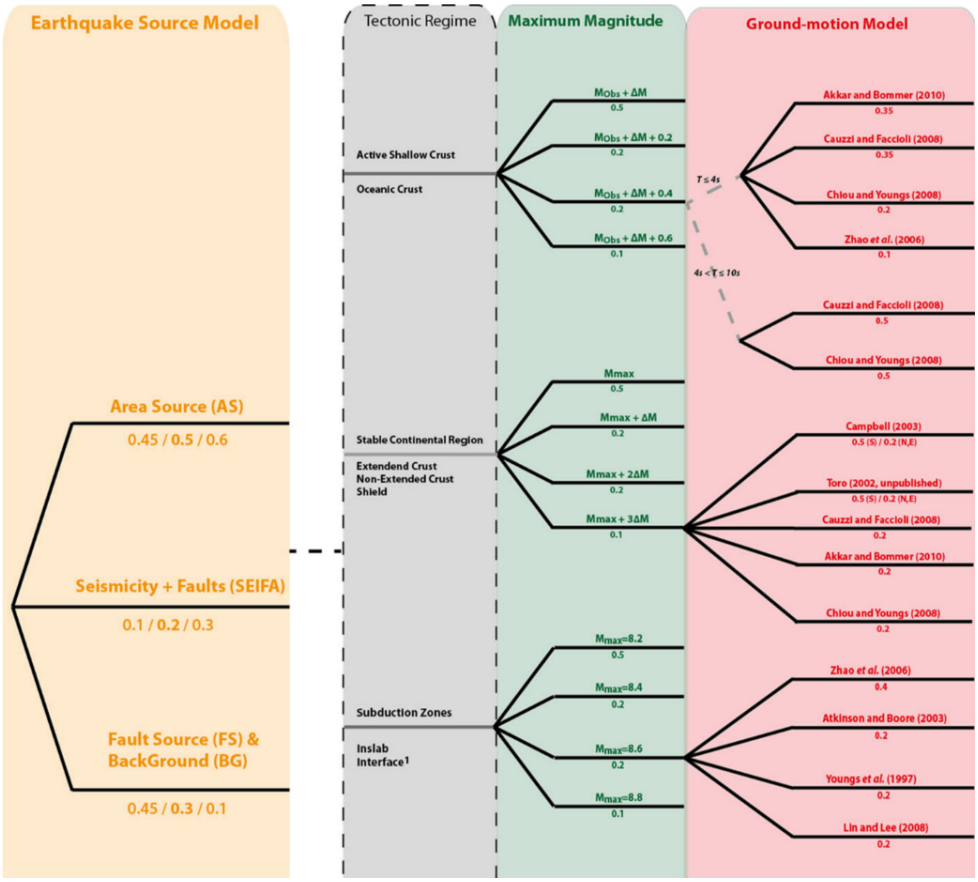

motion, value.

Figure 8. ***ESHM13 logic tree truncated from Figure 5 in Woessner et al. (2015). Colours depict the branching levels for the earthquake source models (yellow), maximum magnitude models (green) and ground motion models (red). Values below the black lines indicate the weights, for the source model these indicate the weighting scheme for different return periods where the middle is for 475 years. Tectonic regionalisation is not a branching level (grey) of the model; however, it defines the GMPEs to be used.***

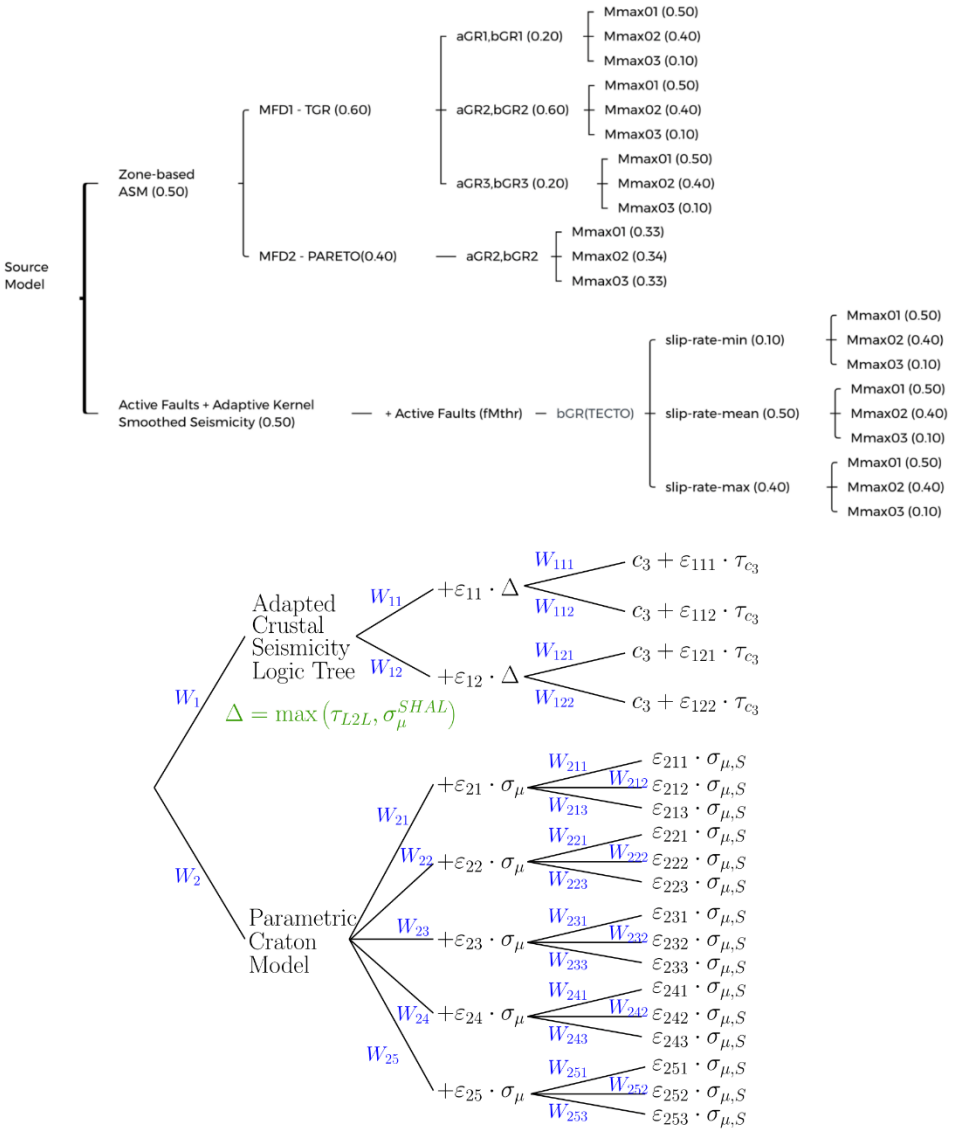

Figure 9. ***ESHM20 logic tree from Figures 3.13 and 4.10 in Danciu et al. (2021). The upper figure shows the logic tree for seismogenic sources of shallow crustal earthquakes, where weights on the branches are indicated by the numbers in parenthesis. The lower figure shows the ground motion logic tree for the stable cratonic region of Fennoscandia, where weights W1 = 0.2, W2= 0.8, W11, W111, W121=0.667, W12, W112, W122=0.333. The W2x weights are assigned a 5-branch discrete approximation of the Gaussian distribution and the W2xy weights a 3-branch discrete approximation.***

Figure 9 shows the main components of the ESHM20 logic tree for shallow crustal earthquakes in the stable cratonic region of Fennoscandia. The seismic source models are divided 50-50 between the area source models (ASM) and the smoothed seismicity approach, in Fennoscandia without defined active faults. In the ASMs there is one branch for the double truncated Gutenberg-Richter calculation of recurrence parameters, with three subbranches to account for uncertainties in a- and b-vales, and a single branch for the Pareto distribution method for a- and b-value estimation. Each of the recurrence parameter branches finally has three associated maximum magnitude branches. The 50-50 division between the area source zones and the smoothed seismicity model implies that the

erroneous recurrence values for area source zone SEAS409 (Ringhals) is limited to a 50% effect on the calculations.

The ESHM20 GMM logic tree for cratonic regions such as the Fennoscandian Shield is depicted in the lower part of Figure 9. The GMM logic tree has one branch, with weight 0.2, with the Shallow Default crustal GMM, albeit not using the low stress or highly attenuating parts of that GMM (Adapted crustal seismicity logic tree in Figure 9). The Craton part of the GMM has weight 0.8 and has two branching levels which are considered to reflect both the epistemic uncertainty in the median ground motion on very hard rock ($\sigma\mu$) and the epistemic uncertainty in the site amplification factor ($\sigma\mu$,S). The former is weighted by a 5-branch discrete approximation of the Gaussian distribution, while the latter has a 3-branch discrete approximation (Danciu et al. 2021). For the non-cratonic areas of Fennoscandia, ESHM20 uses the regular Shallow Default GMM logic tree, which has complexity similar to the Craton GMM, see Weatherill et al. (2020).

The differences between the logic trees of ESHM13 and ESHM20 adds to the complexity of determining why, and how, the two hazard models are different.

3.4. HAZARD RESULTS

Figure 10 shows the seismic hazard in Fennoscandia in terms of the mean peak ground acceleration (PGA) for a 4975-year return period for ESHM13 and for a 5000-year return period for ESHM20, both equal to a 1% exceedance probability in 50 years or a 0.0002 annual exceedance probability. The maps show how the relatively high hazard along the Norwegian west coast has decreased significantly from ESHM13 to ESHM20 and that also southern Norway and the Swedish west coast has decreased hazard in ESHM20. Conversely, southcentral Sweden and the Swedish northeast coast see increased hazard in ESHM20, as does the Finnish Kuusamo region. Mapping the difference between the two models at 5000-year return period, Figure 11 shows that southwestern Norway has a decrease in PGA of up to 0.25 g, that the Swedish southwest coast has decrease in PGA of about 0.1 g and that the PGA in southern Finland and southcentral Sweden increase by up to 0.05 g in ESHM20 compared to ESHM13. We note that on a regional scale, the differences in Figure 11 shows a resemblance to the GMM areas of Shallow Default and Craton. The implications of these differences for the NPP sites are investigated more thoroughly in Section 3.5.

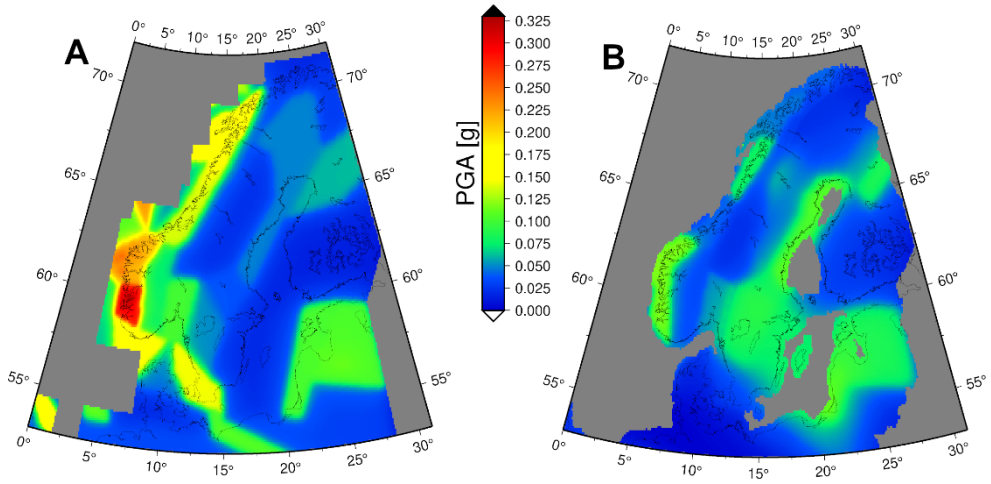

Figure 10. ***Maps displaying the mean peak ground acceleration values in units of g. A) ESHM13 for a 4975-yr return period, B) ESHM20 for a 5000-yr return period. Data from https://www.efehr.org/***

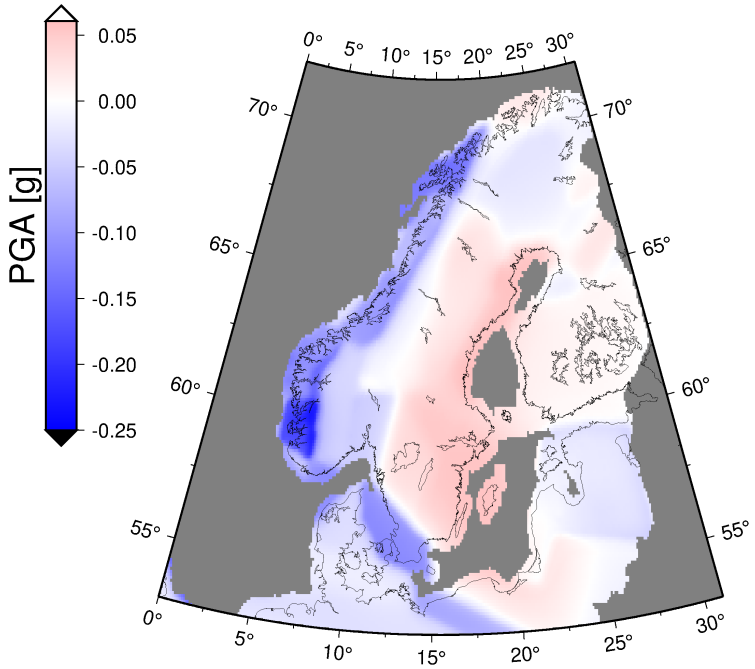

Figure 11. ***Map displaying the difference in mean peak ground acceleration, in units of g, between ESHM20 and ESHM13 for a 5000-year return period. Red colours indicate higher values in ESHM20, blue colours indicate lower values in ESHM20. Data from https://www.efehr.org/***

3.5. HAZARD DIFFERENCES AT THE NUCLEAR POWER PLANT SITES

Following the general differences between ESHM13 and ESHM20 outlined above, the seismic hazard at all nuclear power plant (NPP) sites except at Ringhals has increased. In this section we will evaluate these differences in more detail and try to assess their significance.

3.5.1. Methodologies to assess differences

Douglas et al. (2023) conducted a comprehensive literature review, identifying four studies where the issue of comparison of pairs of seismic hazard models and examination of their differences was addressed. The first approach is proposed by McGuire (2012) and suggests that if an updated hazard model changes the mean Annual Frequency of Exceedance (AFE) by more than 25% for ground-motions corresponding to a mean AFE of 10-4 in the original model, and similarly changes the mean AFE by more than 35% for ground-motions corresponding to a mean AFE of 10-6 in the original model, then the change should be considered significant.

The second approach, based on Cohen's (1977) effect size, is proposed by Malhotra (2014, 2015). It uses the ground-motion Probability Density Functions (PDFs) derived from the hazard models to calculate the Cohen's effect size:

$$d = \frac{\mu_1 - \mu_2}{\sqrt{0.5(\sigma_1^2 + \sigma_2^2)}} \quad (1)$$

where μ_1, μ_2, σ_1 and σ_2 are the means and standard deviations of the PDFs, respectively. A difference between the compared PDFs is considered large, when Cohen's effect size, d, is greater than 0.8.

The third and fourth approaches for assessing the robustness of a change in hazard between original and updated hazard models are proposed by Abrahamson (2017). His first proposal was that the change is considered robust if the mean hazard for the AFE of interest (i.e., from ESHM13) is outside the 25th and 75th ground-motion fractiles of the updated hazard model (ESHM20). Since the 25th and 75th fractiles are not computed in the ESHMs, deriving the ground-motion PDF of the updated hazard model is needed for the application of this approach. In the second proposed approach by Abrahamson (2017), the change is considered robust if the criterion described by the following inequality is met:

$$\ln\left(\frac{IM_{new}}{IM_{old}}\right) - 0.5\sigma_{haz} > 0 \quad (2)$$

where IM_{old} and IM_{new} are the mean ground-motion levels at the AFE of interest and σ_{haz} is the standard deviation derived from the logarithms of the fractiles at the target AFE.

3.5.2. Deriving a probability density function from fractiles

A standardized PDF of a normal distributed continuous random variable is defined by

$$f(x) = \frac{e^{(-x^2/2)}}{\sqrt{2\pi}} \quad (3)$$

This standardized distribution can be shifted and/or scaled using the loc and scale parameters by:

$$f(x) = \frac{e^{-0.5\left(\frac{x-loc}{scale}\right)^2}}{scale\sqrt{2\pi}}, \quad (4)$$

and the Cumulative Distribution Function (CDF) can be obtained by integrating the PDF:

$$F(x) = \int_{-\infty}^{x} f(t)dt \quad (5)$$

In a normal distribution, the loc parameter is the mean or expectation of the distribution which is equal to the distribution's median and mode. The scale parameter represents the standard deviation of the normal distribution.

A fractile represents a specific cut-off point within a distribution where the cumulative probability reaches a predetermined level. For example, the 14th fractile marks the value below which there is a cumulative probability of 14%, while the 84th fractile denotes the value below which there is a cumulative probability of 84. The loc and scale parameters can be calculated using the fractiles:

$$scale = \frac{x_2 - x_1}{F^{-1}(p_2) - F^{-1}(p_1)} \quad (6)$$

$$loc = \frac{x_1 F^{-1}(p_2) - x_2 F^{-1}(p_1)}{F^{-1}(p_2) - F^{-1}(p_1)} \quad (7)$$

where $x_1$and x_2 are the values with probabilities $p_1$and p_2, and $F^{-1}(p)$ is the inverse CDF of the normal distribution.

A PDF of a lognormally distributed variable, y, can also be described using the *loc and scale* parameters:

$$f(y) = \frac{1}{scale\sqrt{2\pi}y} e^{-0.5\left(\frac{\log(y)-loc}{scale}\right)} \quad (8)$$

However, in the lognormal distribution, the loc and scale parameters should not be mistaken for mean and standard deviation as the descriptive statistics of a normal distribution.

The lognormal distribution of a random variable, x, can also be seen as the normal distribution of $\log(x)$. Therefore, the statistics describing a lognormal distribution can be derived by $f(\log(x))$. Given the logarithm of the values with certain probabilities (e.g., 16% and 84%), one can estimate the standard deviation of the

lognormal distribution either using $f(\log(x))$ derived from the fractiles or $0.5\log(x^{84\%}/x^{16\%})$.

If the lognormally distributed random variable, x, is transformed to a normal distribution using $\log(x)$, the loc and scale parameters can then be viewed as the mean and standard deviation of the transformed random variable.

3.5.3. Assessment of the differences

The peak ground motion levels in hazard results are lognormally distributed. The mean, median and some fractile (e.g., 15th, 16th, 85th and 84th) hazard curves are computed in the ESHM13 and ESHM20 models (Woessner et al. 2015; Danciu et al. 2021, 2024). The mean, median and fractile hazard curves for the five NPP sites of interest in Finland and Sweden (Figure 1) are shown in the top rows of Figures 12-16. However, estimation of the standard deviations and 25th and 75th fractiles are needed for the implementation of the comparison approaches proposed by Malhotra (2014, 2015) and Abrahamson (2017) (see section 3.5.1). To this end, the lognormal distributions of the hazard models are derived from the reported 15th,16th, 84th and 85th fractiles by implementation of the theoretical background introduced in section 3.5.2. The lognormal distributions are utilized for calculation of the fractiles needed for the first approach introduced by Abrahamson (2017) (i.e., 25th and 75th). We also used the lognormal PDFs to estimate the standard deviations needed for the approach introduced by Malhotra (2014, 2015), as well as for the second approach of Abrahamson (2017). The necessary mean hazard values are used directly from the reported ESHM13 and ESHM20 curves rather than from our constructed PDFs. The lognormal PDFs of PGA values for the return periods of 475, 2475, 5000, 104 and 106 years are illustrated in the lower parts of Figures 12-16. The 25th and 75th fractiles are marked by vertical lines and estimated lognormal standard deviations are mentioned. The first proposed method of Abrahamson (2017) can be visually inspected by comparing the location of blue circles (the mean hazard from ESHM13) and vertical red lines (the 25th and 75th fractiles from ESHM20). Results of the four comparison methodologies assessing the importance of variations between ESHM13 and ESHM20 across five NPP sites in Sweden and Finland, accounting for different return periods, are presented in Table 2. Consistent terminology from the original works is retained to describe the importance.

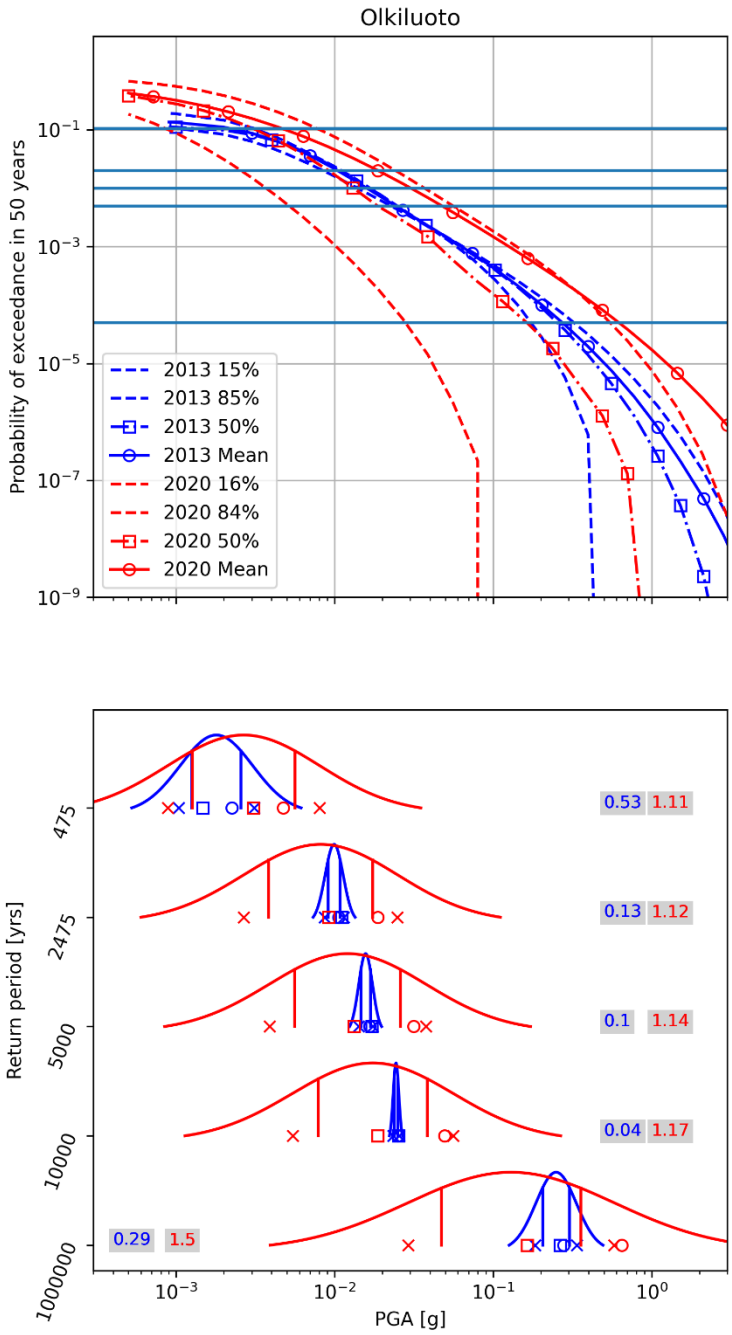

Figure 12. ***(Upper) Mean, median and two fractile hazard curves for the Olkiluoto NPP site from ESHM13 and ESHM20 illustrating the probability of exceedance in 50 years. The blue horizontal lines indicate the return periods of 475, 2475, 5000, 10^4 and 10^6 years. (Lower) The PDFs derived from the hazard models for return periods of 475, 2475, 5000, 10^4 and 10^6 years. Mean and median PGA values associated with each model are adapted from the original curves and are marked by circles and squares, respectively. The fractiles originally provided by the hazard models are shown by crosses. 25th and 75th fractiles estimated from the fitted lognormal distributions are shown by vertical lines. Colored numbers are the standard deviations estimated from the fitted PDFs.***

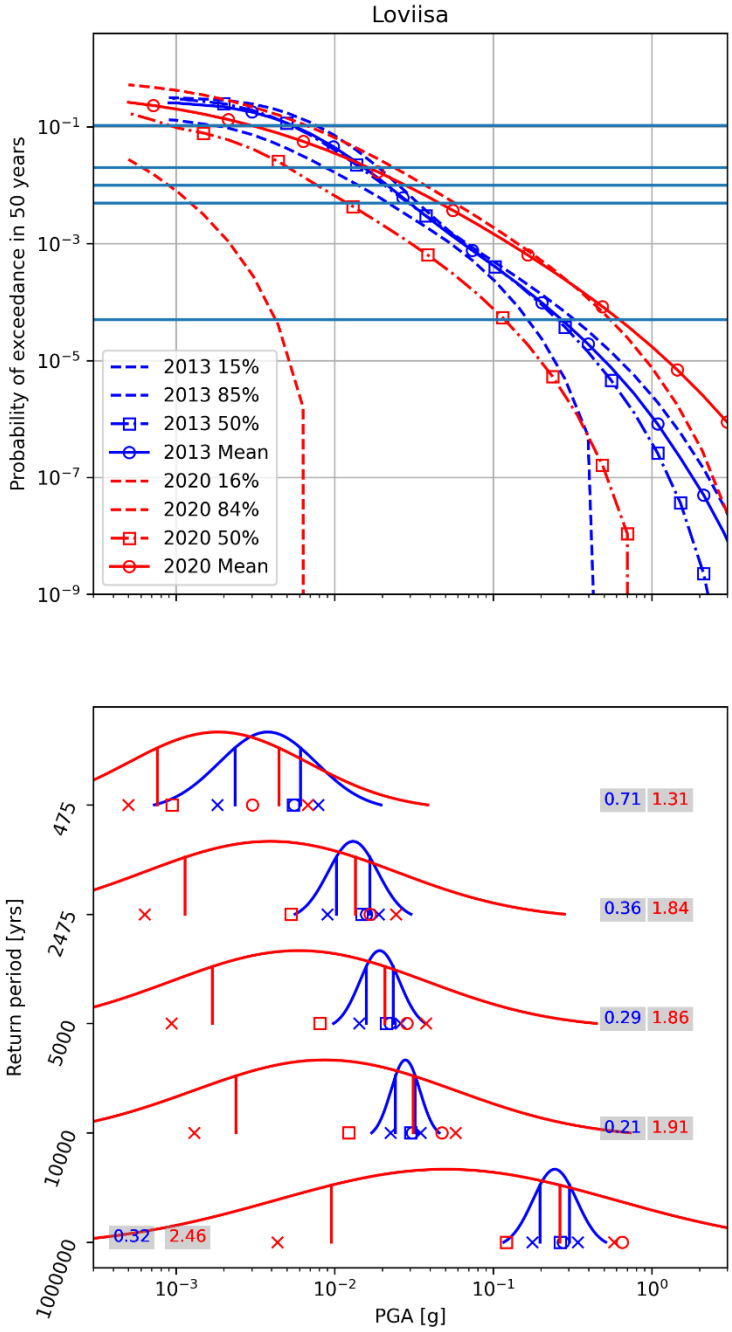

Figure 13. ***(Upper) Mean, median and two fractile hazard curves for the Loviisa NPP site from ESHM13 and ESHM20 illustrating the probability of exceedance in 50 years. The blue horizontal lines indicate the return periods of 475, 2475, 5000, 10^4 and 10^6 years. (Lower) The PDFs derived from the hazard models for return periods of 475, 2475, 5000, 10^4 and 10^6 years. Mean and median PGA values associated with each model are adapted from the original curves and are marked by circles and squares, respectively. The fractiles originally provided by the hazard models are shown by crosses. 25th and 75th fractiles estimated from the fitted lognormal distributions are shown by vertical lines. Colored numbers are the standard deviations estimated from the fitted PDFs.***

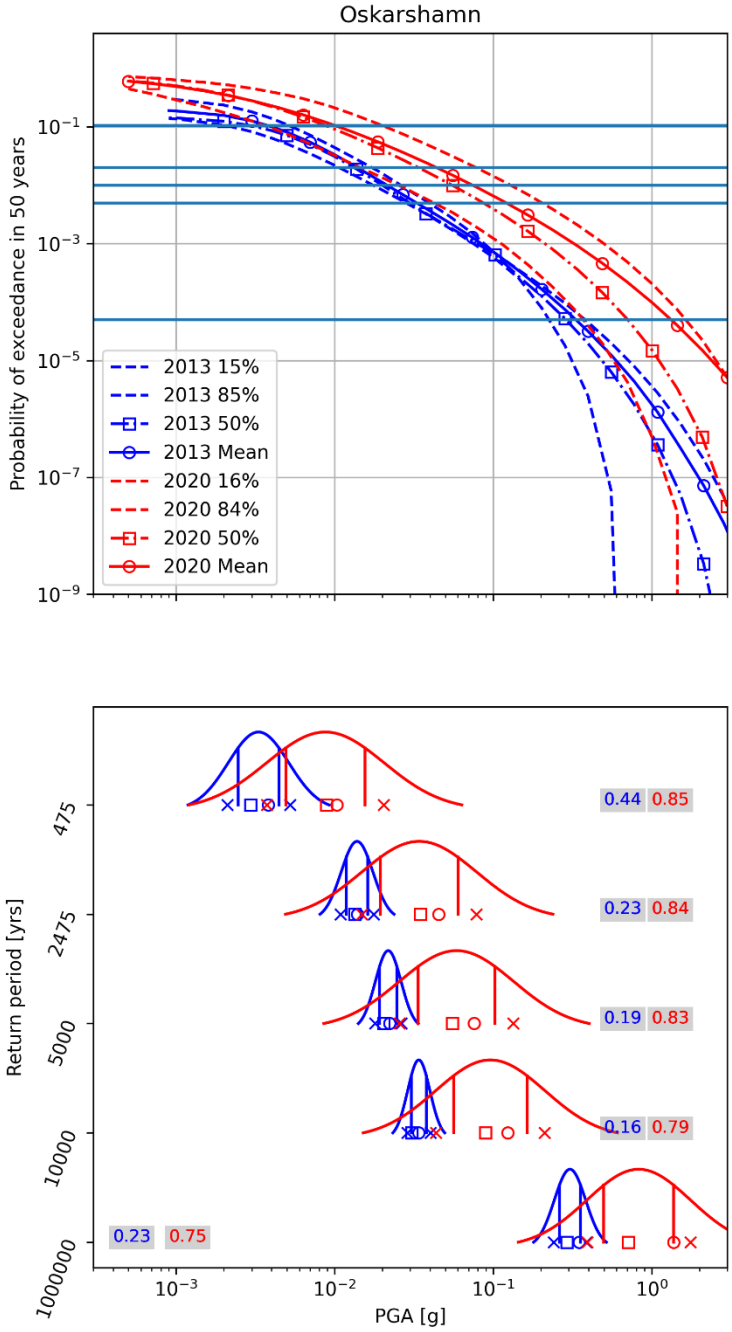

Figure 14. ***(Upper) Mean, median and two fractile hazard curves for the Oskarshamn NPP site from ESHM13 and ESHM20 illustrating the probability of exceedance in 50 years. The blue horizontal lines indicate the return periods of 475, 2475, 5000, 10^4 and 10^6 years. (Lower) The PDFs derived from the hazard models for return periods of 475, 2475, 5000, 10^4 and 10^6 years. Mean and median PGA values associated with each model are adapted from the original curves and are marked by circles and squares, respectively. The fractiles originally provided by the hazard models are shown by crosses. 25th and 75th fractiles estimated from the fitted lognormal distributions are shown by vertical lines. Colored numbers are the standard deviations estimated from the fitted PDFs.***

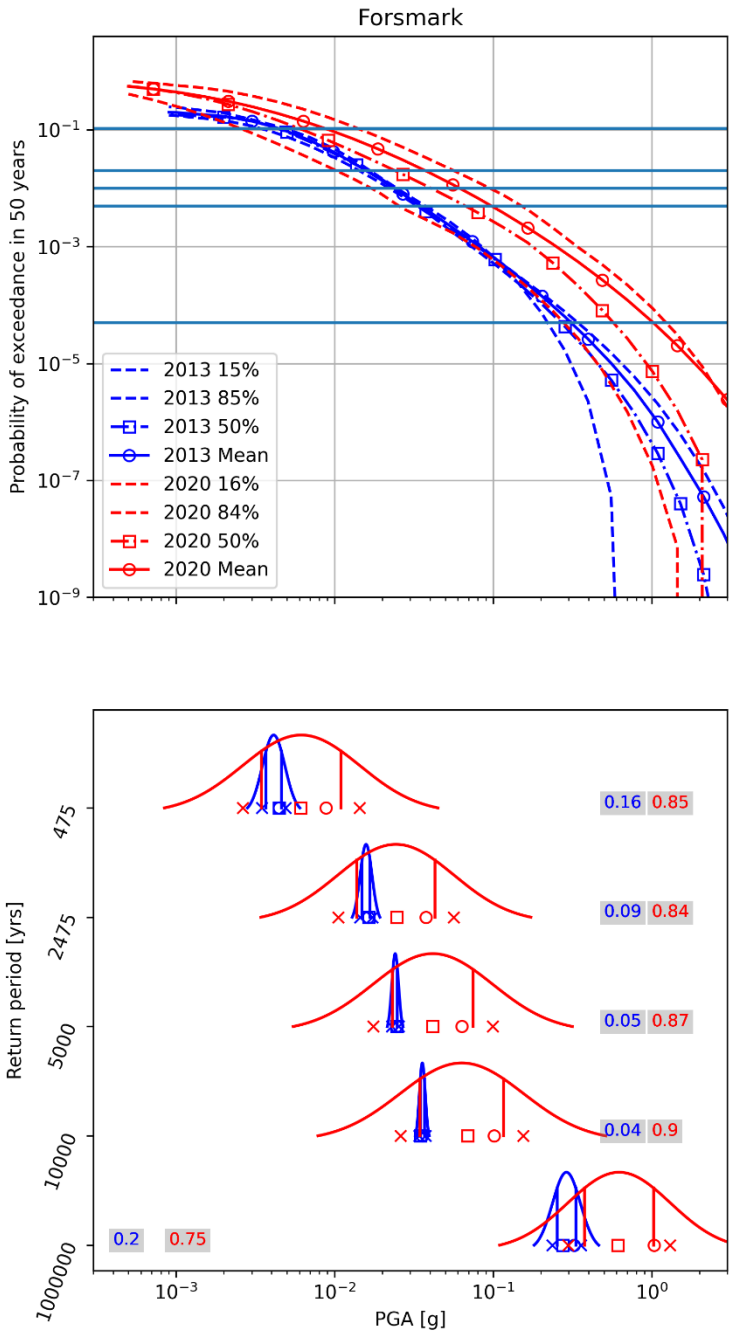

Figure 15. ***(Upper) Mean, median and two fractile hazard curves for the Forsmark NPP site from ESHM13 and ESHM20 illustrating the probability of exceedance in 50 years. The blue horizontal lines indicate the return periods of 475, 2475, 5000, 10^4 and 10^6 years. (Lower) The PDFs derived from the hazard models for return periods of 475, 2475, 5000, 10^4 and 10^6 years. Mean and median PGA values associated with each model are adapted from the original curves and are marked by circles and squares, respectively. The fractiles originally provided by the hazard models are shown by crosses. 25th and 75th fractiles estimated from the fitted lognormal distributions are shown by vertical lines. Colored numbers are the standard deviations estimated from the fitted PDFs.***

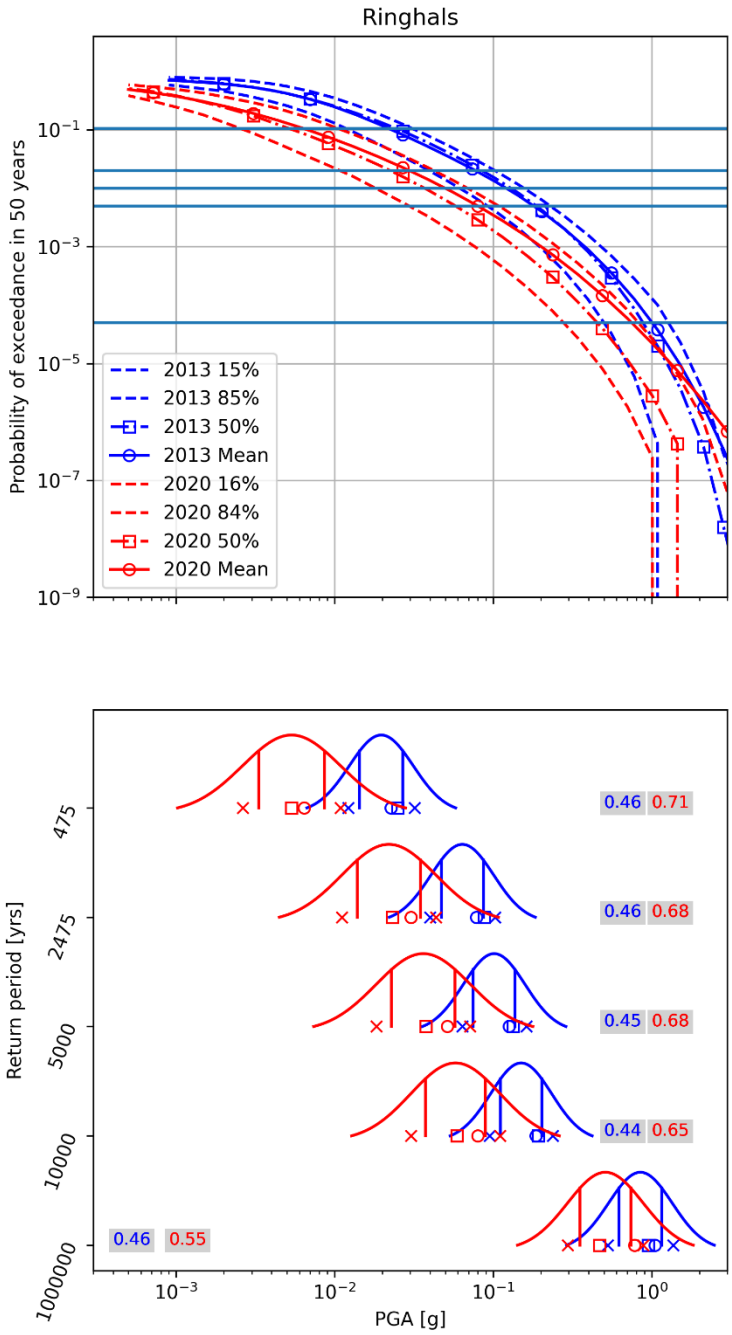

Figure 16. ***(Upper) Mean, median and two fractile hazard curves for the Ringhals NPP site from ESHM13 and ESHM20 illustrating the probability of exceedance in 50 years. The blue horizontal lines indicate the return periods of 475, 2475, 5000, 10^4 and 10^6 years. (Lower) The PDFs derived from the hazard models for return periods of 475, 2475, 5000, 10^4 and 10^6 years. Mean and median PGA values associated with each model are adapted from the original curves and are marked by circles and squares, respectively. The fractiles originally provided by the hazard models are shown by crosses. 25th and 75th fractiles estimated from the fitted lognormal distributions are shown by vertical lines. Colored numbers are the standard deviations estimated from the fitted PDFs.***

Table 2. Importance of variations between ESHM13 and ESHM20 evaluated by four hazard comparison methodologies at five NPP sites in Sweden and Finland, accounting for

different return periods. Consistent terminology from the original works is employed to describe the importance.

Return Period	10^6	10^4	5000	2475	475
Ringhals					
McGuire*	Significant	Significant	-	-	-
Abrahamson#	Robust	Robust	Robust	Robust	Robust
Abrahamson×	Non-robust	Non-robust	Non-robust	Non-robust	Non-robust
Malhotra|	Not large	Not large	Not large	Not large	Not large
Forsmark					
McGuire*	Significant	Significant			
Abrahamson#	Robust	Non-robust	Non-robust	Non-robust	Non-robust
Abrahamson×	Robust	Robust	Robust	Robust	Robust
Malhotra|	Large	Not large	Not large	Not large	Not large
Oskarshamn					
McGuire*	Significant	Significant	-	-	-
Abrahamson#	Robust	Robust	Robust	Robust	Robust
Abrahamson×	Robust	Robust	Robust	Robust	Robust
Malhotra|	Large	Not large	Not large	Not large	Not large
Loviisa					
McGuire*	Significant	Significant	-	-	-
Abrahamson#	Robust	Non-robust	Robust	Robust	Robust
Abrahamson×	Non-robust	Non-robust	Non-robust	Non-robust	Non-robust
Malhotra|	Not large	Not large	Not large	Not large	Not large
Olkiluoto					
McGuire*	Significant	Significant	-	-	-
Abrahamson#	Non-robust	Non-robust	Non-robust	Non-robust	Non-robust
Abrahamson×	Robust	Robust	Robust	Robust	Robust
Malhotra|	Not large	Not large	Not large	Not large	Not large

*Based on the criterion proposed by McGuire (2012); #Based on the first criterion proposed by Abrahamson (2017); ×Based on the second criterion proposed by Abrahamson (2017); |Based on the criterion proposed by Malhotra (2014, 2015)

3.5.4. Coefficient of variation

The coefficient of variation (COV) in statistics is a measure of the dispersion of a probability distribution and frequently used in PSHA. It is defined simply as the

ratio between the standard deviation and the mean. As an example, Malhotra (2015) uses COV to compare PSHA results from the USGS for Los Angeles and infers that over four iterations of hazard assessments, COV and consequently the uncertainty in the results, constantly increase. In Table 3 the mean, standard deviation and COV from ESHM13 and ESHM20 at the NPP sites is exemplified using the PGA at $2 \cdot 10^{-4}$ annual exceedance probability, or 5000-year return period, the longest where ESHM13 and ESHM20 claim validity (Woessner et al., 2015; L. Danciu, private communication, 2023). The mean has been extracted from the hazard curves and the standard deviation calculated as above.

Table 3 shows that the difference in hazard between ESHM20 and ESHM13 for the NPPs is large compared to the estimated mean hazard. The mean hazard has increased at Oskarshamn by 0.053 g, Forsmark 0.038 g, Olkiluoto 0.014 g, Loviisa 0.007 g whereas it has decreased at Ringhals by 0.07 g. Table 3 also shows that the standard deviations have generally increased significantly, as could be observed in the figures in Subsection 3.5.3. The change in COV shows that the increase in standard deviations is significantly larger than the increase in the means, such that the COV has increased by factors of 1.2 to 6.7. At Ringhals, the decrease in the mean also contributes to a higher COV. The COVs at the Finnish NPPs are significantly higher than at the Swedish NPP sites in ESHM20.

Table 3. Hazard (PGA) mean, standard deviation (σ) and coefficient of variation (COV) for a return period of 5000 year for the five nuclear power plant (NPP) sites in ESHM13 and ESHM20.

	ESHM13			ESHM20		
NPP	mean	σ	COV	mean	σ	COV
Forsmark	0.024	0.056	2.3	0.062	0.87	14.0
Ringhals	0.12	0.45	3.8	0.050	0.68	13.6
Oskarshamn	0.021	0.19	9.0	0.074	0.83	11.2
Olkiluoto	0.016	0.091	5.7	0.030	1.14	38.0
Loviisa	0.022	0.29	13.2	0.028	1.86	66.4

3.5.5. Remarks

At first glance, a visual inspection of the PDFs derived from the ESHM13 and ESHM20 models (Figures 12-16) reveal that for all the return periods, the PDFs estimated from ESHM20 are much wider than those from ESHM13 at all NPP sites, except at Ringhals. This is also evident in the increase in COV for all sites. Examples of tight distributions are especially clear at the Forsmark NPP site for return periods of 5000 and 10^4 years (Figure 15) and at the Olkiluoto site for the return period of 10^4 years (Figure 12). Such remarkable increases in the standard deviations from ESHM13 to ESHM20 places the mean hazard from ESHM13 inside

the 25th to 75th ground-motion fractiles of ESHM20 at these sites, resulting in the change not considered robust at Forsmark and Olkiluoto, according to the first criterion of Abrahamson (2017).

Ringhals is the only NPP site where the mean hazard values from ESHM20 are smaller than those from ESHM13 at all the return periods of interest (Figure 16). Such a decrease in hazard level from ESHM13 to ESHM20 is also observable at the Loviisa site for the return periods shorter than approximately 2500 years (Figure 13). This reduction in hazard values from ESHM13 to ESHM20 at the Ringhals site is the underlying cause of the change not being considered robust, based on the second criterion of Abrahamson (2017). However, according to the same criterion, the non-robust changes at the Loviisa site are caused by significantly high values of standard deviations of ESHM20.

The Cohen (1977)'s effect size, which increases with the difference in mean hazards and deceases with larger standard deviations, serves as the foundation for the criterion put forth by Malhotra (2014, 2015). Hence, the significant standard deviations linked to the ESHM20 model contribute to an enlargement of the denominator in Equation (1), consequently yielding a reduced Cohen (1977)'s effect size. This explains why the criterion suggested by Malhotra (2014, 2015) is not satisfied in the majority of cases.

Neither of the two methods suggested by Abrahamson (2017) constitutes a formal statistical test, and it remains unclear how to interpret the contradictory results arising from these approaches. As is highlighted by Douglas et al. (2023), the methodologies proposed by Malhotra (2014, 2015) and Abrahamson (2017) rely on variations in ground-motion levels corresponding to a given return period. This approach is commonly employed in practical applications, such as regional and national hazard maps, to ascertain the ground-motion level for a specific return period of interest. Although hazard results are typically used in this manner, the hazard engines provide AFE for a given ground-motion level. The approach proposed by McGuire (2012) acknowledges this by utilizing AFEs in his criteria. This aligns with how hazard models can be employed in risk assessment through the convolution of hazard and fragility/vulnerability curves. Therefore, opting for the differences in AFE at a specified ground-motion level may be more reasonable.

When analyzing the implications of the methods (Table 2), McGuire's (2012) approach, as the most risk-oriented among the four employed methods, emphasizes the significance of the differences across all NPP sites and long return periods (10^4 and 10^6 years). Conversely, the two criteria proposed by Abrahamson (2017) yield conflicting results in four out of five NPP sites (Oskarshamn is the only exception), with only one of the approaches (either the first or the second approach) underscoring the importance of disparities between the compared hazard models. Douglas et al. (2023) have cautioned that the second approach (Equation 2) suggested by Abrahamson (2017) might yield misleading results in low-hazard areas. The application of the Malhotra (2014, 2015) criterion generally reveals small differences between the models, partly due to the standard deviations in ESHM20 being large relative to the differences in the mean. All in all, across all NPP sites, a minimum of two out of the four comparison methodologies suggests significant changes between the ESHM13 and the ESHM20 models for the

return period of 10^6 years, signifying the importance of these differences towards the longer periods. The comparison approach proposed by McGuire (2012) is only meant to be used for the longer return periods (10^4 and 10^6 years) and therefore it is not applied to the return periods shorter than 10^4. Among the other methodologies applied to the return periods of 475, 2475 and 5000 years, a minimum of one approach suggests significant changes between the ESHM13 and the ESHM20 models.

4. Seismic hazard components for Fennoscandia

Figures 8 and 9 in Section 3.3 give a glimpse of the complexity of the logic trees in ESHM13 and ESHM20, respectively. However, not all the branches of the pan-European work are relevant for Fennoscandia. The logic tree is also of practical value, since it documents and displays in a transparent fashion the state of seismotectonic data and geoscientific perception in the target region. The number of nodes increases with data availability; for example, the number of fault segments of a mapped active fault that can break in a future earthquake constitute a node with the respective branches. The various rupture lengths lead to different maximum magnitudes associated with the scenarios. Fault mechanisms and other detailed information about the fault behavior, such as directivity, can also be included. The number of branches may grow significantly, which makes logic trees computationally demanding. In low-seismicity regions such as Sweden and Finland, by contrast, the seismicity of area seismic sources is expressed by only a few parameters. A solitary maximum magnitude distribution is typically assumed to capture all possible vibratory harm from future earthquakes. The main concern is that sufficiently, but not unrealistically, high magnitudes are considered (Mäntyniemi et al. 2023). The resulting logic trees are more pruned than those constructed for active fault seismic sources. Whatever the size of the logic tree, part of any PSHA is to analyze and check the consistency of the results. This section looks at the analysis of the logic tree following Fülöp et al. (2023).

Figure 17 presents an experimental logic tree prepared for the PSHA of three NPP sites in Finland. It was constructed in the SENSEI (SENsitivity study of SEIsmic hazard prediction in Finland) project, conducted under the auspices of the Radiation and Nuclear Safety Authority in Finland (STUK) in 2019–2020 (Mäntyniemi et al. 2021; Fülöp et al. 2023). The focus of the project was on exploring the sensitivity of PSHA in the country. The project aimed to obtain further insight into the PSHA procedure for future PSHA reviews, rather than to provide new, complete PSHA outcomes to be imposed by the regulator.

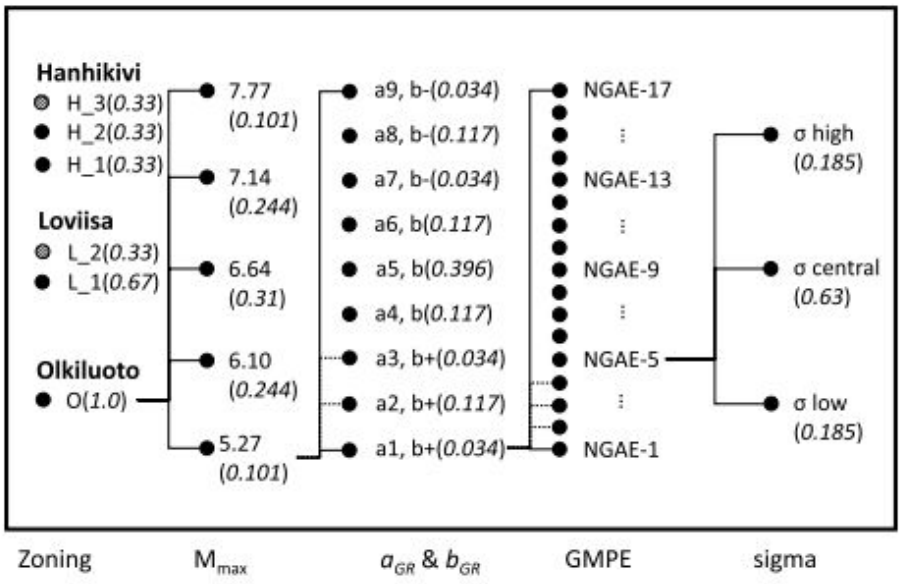

Figure 17 ***Logic tree for Hanhikivi, Loviisa, and Olkiluoto with branching for seismic source zoning, maximum magnitude, the Gutenberg–Richter parameters a and b (b+ with standard deviation added and b− subtracted), the ground-motion prediction equation (GMPE) prediction, and the GMPE randomness (σ) estimate. The black and gray dots represent nodes. The two gray nodes stand for two seismic source zonings prepared in the project. The GMPE nodes refer to the 17 mean predictions of the Next Generation Attenuation – East GMPE, and σ refers to its three ergodic σ models (Goulet et al. 2018; Youngs et al. 2021). The seismic source zoning models H_3 and L_2 are modifications made during the SENSEI project. The weights of the logic-tree branches are shown in the parentheses, except for the GMPEs which are dependent on the spectral frequency and were taken from Table 9-2 of Goulet et al. (2018). Reproduced from Fülöp et al. (2023)***

The final logic trees used had 4590, 2295, and 6885 branches for sites Loviisa, Olkiluoto, and Hanhikivi, respectively (Figure 17). Each logic tree had five branching levels, and the different numbers of branches follow solely from the number of alternative SSZ models available for each site (Fülöp et al. 2023). Besides the zoning models, the branching levels included the maximum magnitude, the Gutenberg–Richter parameters *a* and *b*, the GMPE prediction, and the GMPE randomness (σ) estimate. Half of the nodes are associated with the 17 mean predictions of the NGA-East GMPE and the respective three ergodic sigma (σ) models (Goulet et al. 2018; Youngs et al. 2021).

In the SENSEI project, the distribution of the hazard among the logic-tree branches was analyzed for PGA (taken to be 100 Hz) and 1 Hz at AFE 10^{-5}, the highest and lowest frequency investigated. Not all branches of the logic tree contribute equally to the resulting hazard. Figure 18 shows that the branches generating a higher hazard concentrate at certain nodes that can vary with the spectral frequency. For example, the nodes with a low *b*-value (the three uppermost nodes) contribute to a much higher hazard than those corresponding to a high *b*-value at both frequencies. The different GMPE predictions also contribute differently to the hazard; some of them contribute more strongly to the resulting hazard at both frequencies, while some others contribute more strongly at PGA. The significance of the maximum magnitude also depends on the frequency. Both Loviisa and Olkiluoto are situated in very low-seismicity areas, which presumably explains the

overall similarity of the respective plots in Figure 18. The pattern of the most significant nodes can be quite different for a site with a higher level of nearby background seismicity.

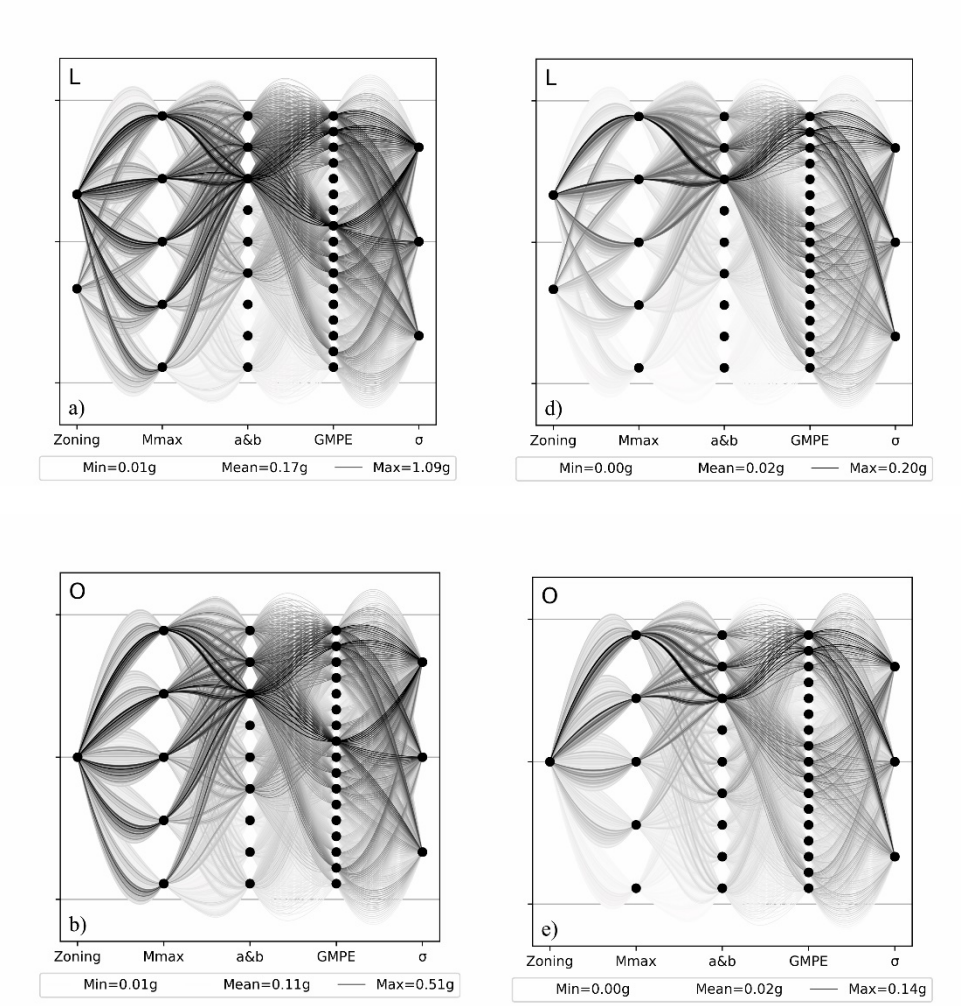

Figure 18. ***Influence of logic-tree nodes on a) b) peak ground acceleration (PGA) and d) e) 1 Hz frequency output for the 10^{-5} annual frequency of exceedance at sites Loviisa (L) and Olkiluoto (O). Line tone represents the hazard on the branch normalized to the maximum value of all branches (i.e., scale is from 0 white to SA_{max}/PGA_{max} black). PGA_{min}, PGA_{max}, and the mean values are given. The nodes (black dots) are retained from Figure 17. Reproduced from Fülöp et al. (2023)***

Figure 19 further illustrates the most important parameters influencing the hazard with the help of so-called tornado plots. The figure has been derived from the hazard curves for 10^{-5} AFE. The values at each branching level represent the spread of hazard observed at that level. The most important parameters influencing the hazard are the ground-motion prediction and the GR parameters. M_{max} is more prominent at the low frequency. Zoning models also have a visible effect for the Loviisa NPP site; only one zoning model was available for Olkiluoto. The two tested zoning models for Loviisa represented a geology-based and seismology-based approach, and were quite different in size. Since much of the observed seismicity occurs in the western part of the Loviisa host zone (this may also be due to data incompleteness in the east), distributing the observed seismicity over a broader or smaller zone leads to very different perception of the hazard. The

delineation of the host zone thus correlates with the seismicity parameters. The a and b values at PGA for Loviisa (Figure 19a) show a very wide spread of the hazard.

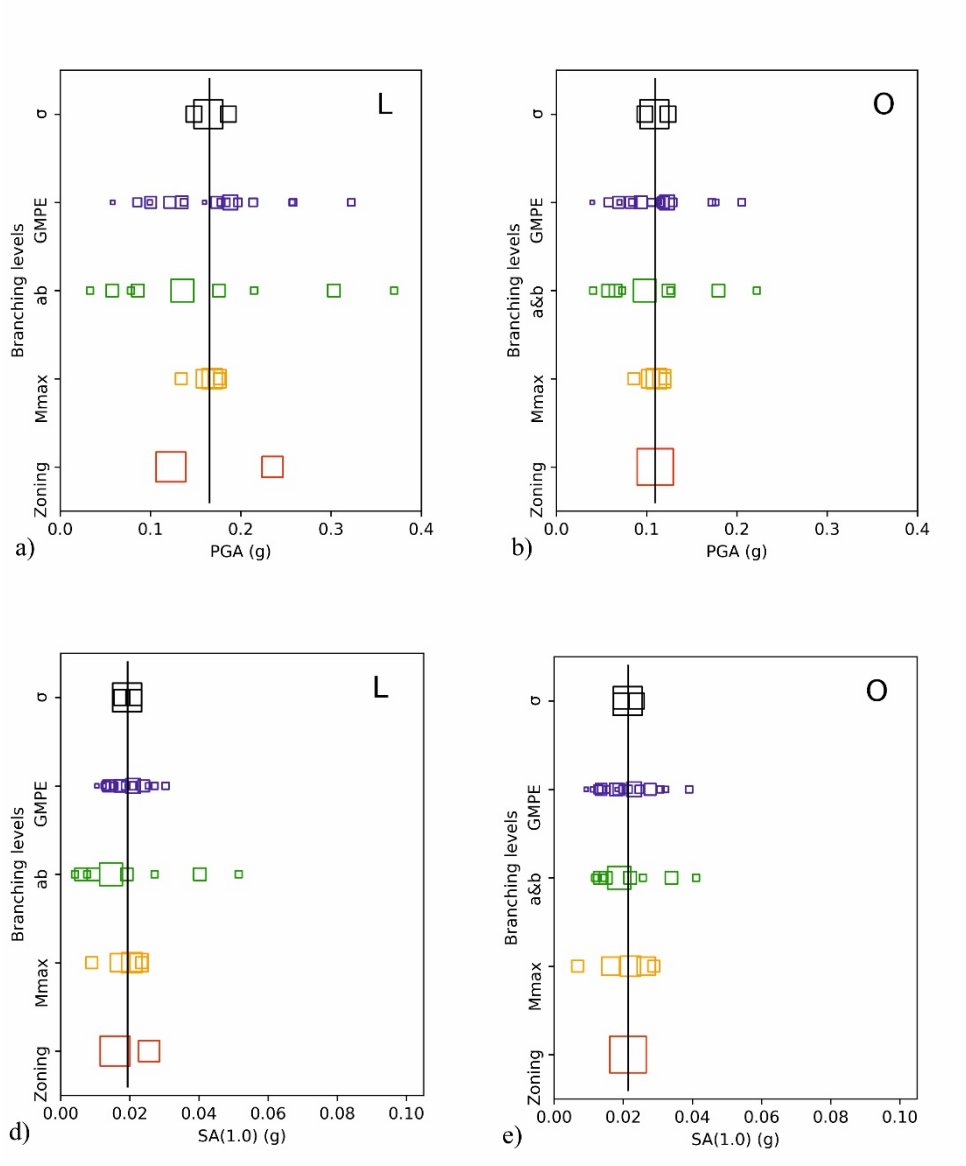

Figure 19. ***Tornado plots of peak ground acceleration (PGA) and 1 Hz spectral amplitude at annual frequency of exceedance 10^{-5} for a) d) Loviisa (L) and b) e) Olkiluoto (O). Branching levels for the zoning maps (red), maximum magnitude (M_{max}) (orange), Gutenberg–Richter a and b parameters (green), ground-motion prediction equation (GMPE; blue), and GMPE randomness (σ) (black). The order of the branching levels is kept the same as in Figures 17 and 18, so the typical tornado shape is not apparent. The square sizes are proportional to the weights of the logic-tree branches included; the weights at each branching level add to unity. The black vertical lines show the mean hazard.*** *Reproduced from Fülöp et al. (2023)*

5. New earthquake data in Fennoscandia

The seismic networks in Fennoscandia have expanded significantly in the 2000s. In Sweden, the Swedish National Seismic Network (SNSN) consisted of five analogue and one digital (Uppsala) seismic station in early 1998. These were modernized and by 2010 the network had expanded to 64 digital broadband stations. A few more have been added since, and a few dismantled, such that in early 2024 the SNSN runs 67 stations, see Figure 20. All stations transmit data in real-time to the center in Uppsala where automatic analysis detects, locates, determines magnitude and classification within 2–3 minutes of an event. The evolution and analysis strategies of the SNSN are described in detail in Lund et al. (2021).

The Finnish National Seismic Network (FNSN) currently consists of over 40 stations out of which the majority is operated by Institute of Seismology, University of Helsinki (ISUH) and nine by Sodankylä Geophysical Observatory, University of Oulu (Kozlovskaya et al. 2016; Figure 20). One of the stations is a small-aperture seismic array (FINES), others are 3-component short-period or broad-band seismograph stations. Data from these stations are integrated in the daily seismic analysis and research at the National Seismological Data Center at ISUH. Since January 2008, the Geological Survey of Estonia has monitored local seismicity in co-operation with ISUH. More information is provided by Veikkolainen et al. (2021) and Soosalu et al. (2022).

The Norwegian seismic network has expanded by 12 stations since 2000. In addition, all stations have been upgraded to 24-bit digitizers and 120 sec broadband sensors, the sampling rate has been increased to 100 samples per second, real-time communication implemented and vaults have been upgraded where necessary (Ottemöller et al. 2021). The Norwegian stations contribute real-time data to automatic detection systems in Fennoscandia.

The Danish seismic network has expanded by five stations in the 2000s and most of the stations have been modernized. Denmark contributes real-time data to automatic detection systems in Fennoscandia.

The densified seismic networks detect significantly more earthquakes today compared to prior to the year 2000. Most of these events are small, below magnitude 3, but they delineate seismically active faults, such as the post-glacial faults in the north, and also illuminate areas of generally higher seismic activity. The data has changed the understanding of the spatial distribution of seismicity (Figure 1) and the seismic activity rates in the low-seismicity intraplate region of Fennoscandia. As is obvious when comparing Figure 1 and Figure 5, there is significantly more data available today than was used for ESHM20. In terms of events with magnitude 3.5 or larger (prior to magnitude homogenization), approximately 30 such events have occurred in our area of interest since the ESHM20 cut-off in 2014. They are almost exclusively located offshore western Norway, except for the June 2015 Mw 3.6 earthquake on the northern Pärvie postglacial fault and the March 2016 Mw 4.1 Bothnian Bay earthquake.

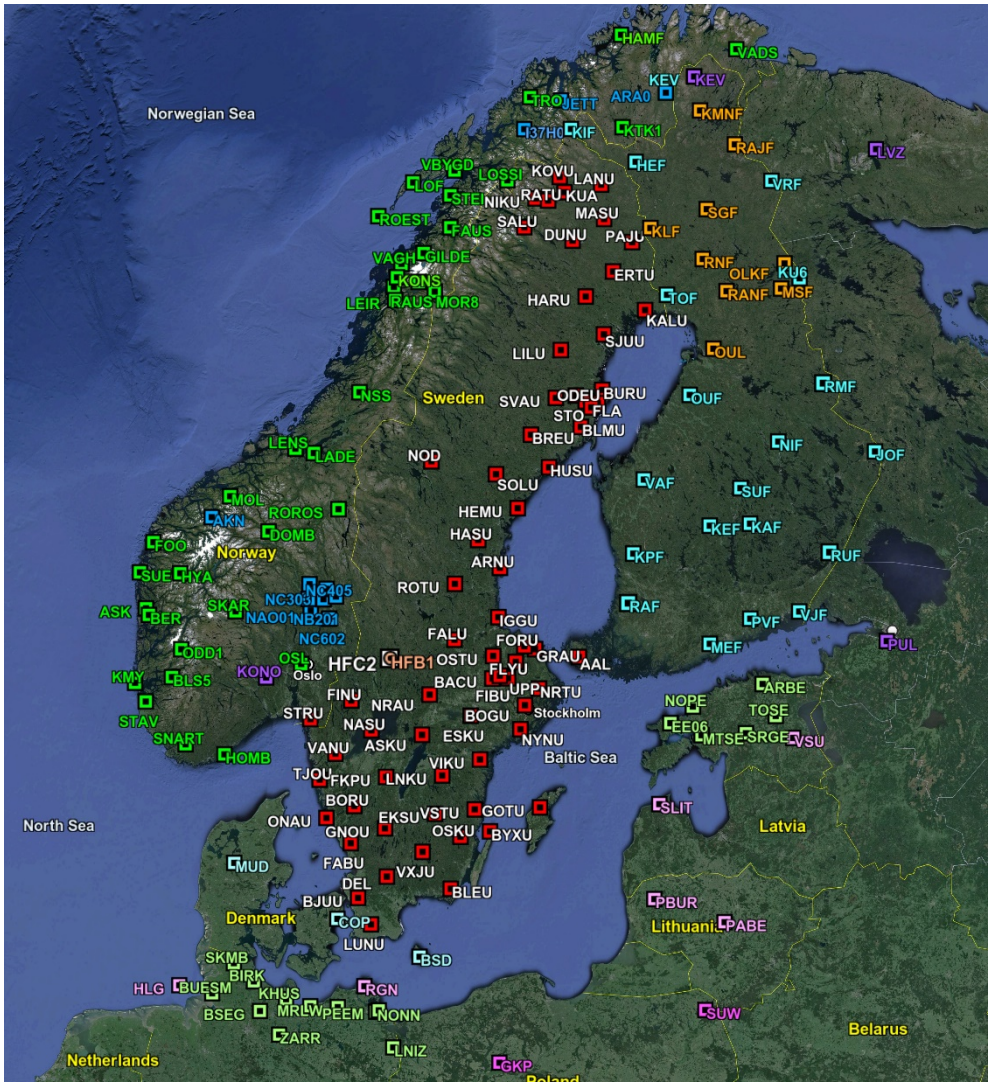

Figure 20 ***Seismic stations in permanent seismic networks in the Fennoscandian and nearby regions. The different colors of the stations indicate different network operators.***

Figure 21 shows the large increase in recorded small events, which accelerated in the 2000s, and that there is now a large amount of data available, albeit unevenly distributed, for the estimation of Gutenberg-Richter recurrence parameters. This implies that an updated hazard assessment can use recurrence parameters calculated for smaller areas, and that there will be areas in Fennoscandia which were almost devoid of events in ESHM20 which can now be properly assessed.

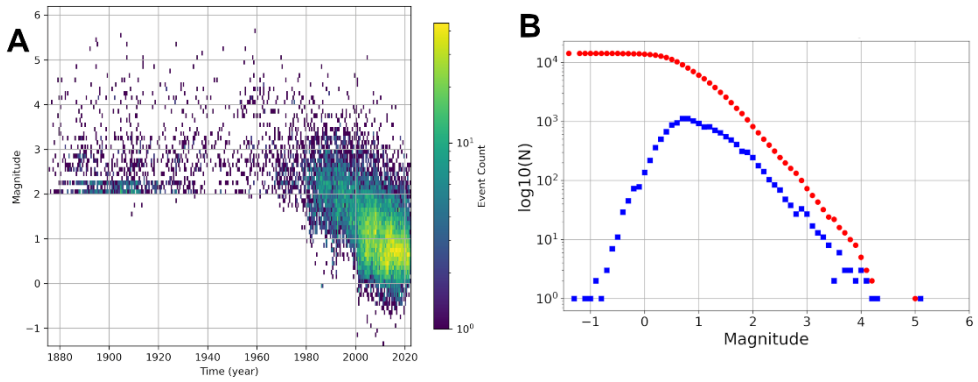

Figure 21. ***An earthquake catalog consisting of a magnitude homogenized and declustered amalgamation of the Fencat and SNSN catalogs for Fennoscandia, excluding data from the mid-Atlantic ridge, the United Kingdom and Russia (Joshi et al. 2023). (A) Density plot of magnitude versus time since 1875. (B) Gutenberg-Richter plot of events in the catalog from 2001 to 2022. Red dots are the cumulative number of events, blue squares the number of events per 0.1 magnitude bin.***

6. Seismic hazard work in Fennoscandia

There has been a renewed interest in seismic hazard assessments in Fennoscandia in the latest decade, both in response to a general increase in awareness of natural hazards but also specifically in response to needs in the nuclear industry in Sweden and Finland (updated regulations, new power plants, SMRs), to new requirements for tailings dams and to earthquake concerns in Norway. In this section, we briefly describe the most relevant projects until early 2024.

Although none of the Nordic seismological institutions were directly involved in the development of ESHM20, Nordic participation was invited in regional review meetings during the latter stage of the project, in 2019. This led to the formation of an ad-hoc Nordic group that provided feed-back to ESHM20, mainly on seismic source zones and earthquake data. The group has continued discussions mainly on harmonized source zone descriptions, earthquake catalogs cleaned from non-earthquake events and magnitude homogenization, convening both at the annual Nordic Seismology Seminars and at dedicated workshops.

Much work has been carried out in Finland since the start of the comprehensive PSHA for the planned new nuclear power plant at Hanhikivi in the 2010s. PSHA reviews for the existing nuclear installations and a number of projects with the nuclear industry, the Nordic Nuclear Safety Research (NKS) and the regulator STUK has resulted in a significant expansion of the knowledge base on seismic hazard. Examples include the GMPE FennoG16 for Fennoscandia (Fülöp et al. 2020), modelling methodology for ground motions (Jussila et al. 2021), and the sensitivity study discussed in Section 4 (Fülöp et al. 2023). A number of these projects have been in close collaboration with especially Swedish and Danish scientists. The project Mitigation of induced seismic risk in urban environments, funded by the Research Council of Finland in 2020–2023, focused on the seismic hazard and risk associated with deep geothermal power stations in metropolitan Finland, thus expanding the investigations into a new energy sector. It was conducted as a research consortium between University of Helsinki, VTT Technical Research Center of Finland and Geological Survey of Finland. The work on seismic hazard also aimed at a modern seismic hazard map of the country. The NKS project on Evaluating Seismic Hazard in the Nordic Countries in the Context of SMRs: Streamlining Approaches for Assessing Earthquake Sources and Activity Rates has been funded for 2024–2025 and continues the close cooperation on seismic hazard topics between the Nordic countries.

In Sweden, seismic hazard work in the last decade has focused mostly on the long-term assessments for the nuclear waste repository at Forsmark, to a significant degree on deterministic seismic hazard assessment. Recent work on return times of large earthquakes at mine tailing dams evolved into a PhD project on the development of a modern seismic hazard map for Sweden. Based on the large amounts of recent earthquake data in Fennoscandia and joint Fennoscandian discussions on seismic source zone delineation and GMMs, the project implemented PSHA calculations following the ESHM20 utilization of the

OpenQuake engine. The results indicate that the inclusion of the intense, low magnitude activity on the post-glacial faults in northern Fennoscandia significantly affects the hazard estimated there, see Figure 22 (Joshi et al. 2023).

In contrast to Sweden and Finland, Norway has implemented the Eurocode 8 building codes into the national regulations and therefore has a stronger stake in a national seismic hazard model. An updated seismic hazard model was launched by Norsar in early 2020, the model is, however, only commercially available and has not been evaluated by the Fennoscandian seismological community. University of Bergen has participated in the Fennoscandian seismic hazard collaboration and work is ongoing there in a PhD project on a new seismic hazard model. Recent investigations of the Stuoragurra post-glacial fault in northern Norway has significant implications for the seismic hazard posed by the post-glacial faults as Olesen et al. (2021) suggest that the Stuoragurra fault ruptured in a magnitude 7 earthquake as recently as 700–4000 years ago.

Denmark has a National annex to Eurocode 8 which was revised in 2020, partly based on the earthquake hazard evaluation by Voss et al. (2015). Current seismic hazard work in Denmark includes assessment for CO2 storage sites and the joint Fennoscandian discussions.

The Fennoscandian collaboration continues with plans for a joint Fennoscandian seismic hazard model, once the national models now under development have been released.

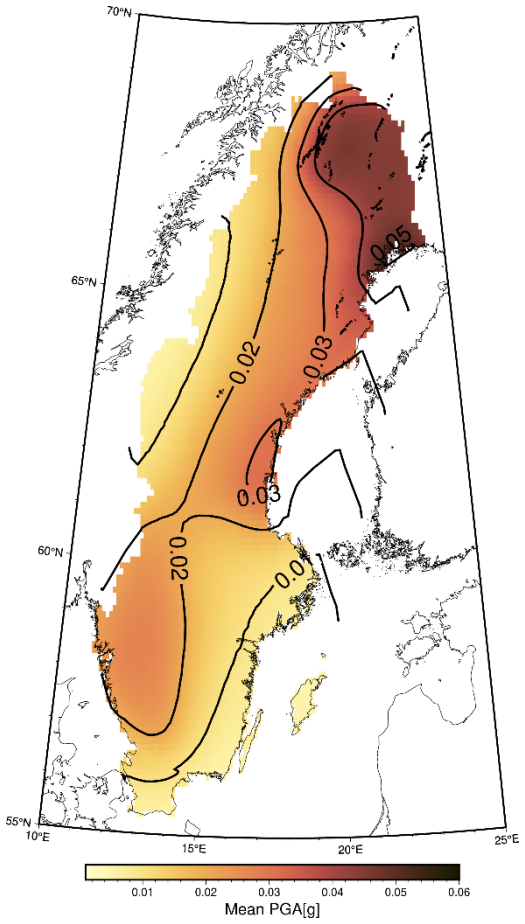

Figure 22. ***A preliminary seismic hazard map of Sweden showing mean peak ground accelerations, in units of g, with a return period of 475 years (Joshi et al. 2023)***

7. Discussion

The ESHM13 and ESHM20 adopted very similar strategies in mapping seismic hazard across Europe and Türkiye (Section 2), but comparing the results of the two models is however no trivial undertaking. The comprehensive analysis of epistemic uncertainty increases the complexity of the logic trees, meaning that the resulting hazard is expressed in terms of distributions across the range of outputs (e.g., Weatherill et al. 2023b). Comparison of the main PSHA components between the two models shows that there are differences not only in the amount of data, but also in the selections and judgments made, as well as in the methodologies used (Section 3). For example, a major difference between the two pan-European models is how the ground motion logic tree was constructed. In the ESHM13 work, a suite of GMPEs was selected, whereas the ESHM20 employed the backbone approach advocated by Douglas (2018). A backbone GMM was specifically developed for cratonic crust by Weatherill and Cotton (2020). It is well recognized that the choice of GMM can have a significant influence on the PSHA results, also shown in Figure 18 (Section 4). Danciu et al. (2021, 2024) also attributed the differences displayed in Figure 4 to various factors, such as differences in modelling assumptions, updated input data and SSZs, a different source model logic tree and ground motion models. We note that the large-scale differences in hazard between ESHM13 and ESHM20 in Fennoscandia, Figure 11, agrees to a large degree with the definitions of Shallow Default and Cratonic GMMs, indicating that the updated GMMs may have a significant influence on the results.

The area source zone SEAS409, encompassing the west coast of Sweden, where the Ringhals NPP is located, and parts of Denmark, has a significantly reduced mean hazard in ESHM20 compared to ESHM13. In Section 3.1 we identified an error in the assignment of recurrence parameters to this zone, which should have inherited a *b*-value of 1.04 from the tectonic zone TSZ007 and used an *a*-value of 2.29, rescaled from TSZ007, but instead has been assigned a *b*-value of 0.84 and an *a*-value of 1.65. The area source zone recurrence parameters are used in the source logic tree with a weight of 50%, and has four branches with the mean and ±1-sigma of the recurrence parameters and a Pareto branch (Figure 9). The remaining 50% in the source logic tree comes from the smoothed seismicity branch, which uses the TSZ007 *b*-value (L. Danciu, private communication, 2024). We saw in Section 3.1 that the erroneous recurrence parameters cause a shorter return time for a magnitude 6.0 earthquake than the correct parameters, which therefore would likely have produced an even lower hazard for Ringhals had they been used.

The ESHM20 has significantly wider PGA distributions than ESHM13 at most return periods and for all compared sites except Ringhals. The Loviisa and Olkiluoto distributions are very wide, as pointed out also by Danciu et al. (2024) in their maps of 95th/5th and 84th/16th fractile ratios. A comparison of the coefficient of variation for the two different models at the NPP sites show that this measure of uncertainty has increased significantly, except at Oskarshamn where the increase is

smaller, mostly due to the widened distributions. The reason for this increase in uncertainty is most likely due to the increased accounting for epistemic uncertainty as expressed by the larger logic trees, especially in a low seismicity region such as Fennoscandia where data, and thus knowledge is scarcer. The wide distributions are therefore not necessarily problematic although a decrease in COV would be appropriate for the next generation models. The wide distributions also imply that not only has the mean hazard, as often expressed in maps, increased in eastern Fennoscandia but also that the high hazard tails (e.g. 95% or higher) of the distributions may extend to PGA values that affect NPP risk estimation.

The different branches of the logic tree represent alternative models or model parameterizations and their associated weights, leading to a number of hazard curves expressing the annual frequency of exceedance (AFE) of the selected ground-motion measures, typically PGA. When PSHA is performed for design purposes, two decisions must be made to obtain values of ground-motion parameters: which AFE should be adopted, and from which hazard curve should the ground-motion value be read (the mean is typically selected). Thus, the different PSHA models also lead to increased or decreased PGA values at specified geographical locations, where the differences must be quantified. The methodologies found in the literature by Douglas et al. (2023) to assess the significance of the differences build on direct comparison between the ground-motion values (McGuire 2012; Abrahamson 2017) or attempt to understand the differences in terms of probability density functions (Malhotra 2014, 2015). The application of these tests to the ESHM13 and ESHM20 data for the five nuclear power plants (Section 3.5) confirmed that assessing the difference between PSHA results is a difficult task (e.g. Malhotra 2015; Douglas et al. 2023). Different tests gave different results when applied to the same data, similar to the results obtained by Douglas et al. (2023) when they applied the tests to PSHA results from Switzerland, Italy and a comparison between ESHM13 and ESHM20 at five different locations. However, the analyses made in Section 3.5 provide insight into the differences. Douglas et al. (2023) conclude that the methods above are not adequate to evaluate formally the statistical *significance* of the difference between two models but that it is vital to consider the uncertainties when comparing hazard results. They also point out that the *importance* of differences between hazard models depends on the application and should be evaluated from a risk perspective.

As the quantitative comparisons between ESHM13 and ESHM20 we have made at the NPP locations are somewhat inconclusive as to the significance of the differences, one may be tempted to ask if ESHM20 is any better than ESHM13? The answer is yes, as the update in ESHM20 adds more data, includes updated models, new methodologies and accounts for more epistemic uncertainties through the logic tree. ESHM20 is therefore the appropriate model to use.

When comparing the execution of the projects leading to the two seismic hazard models, it can be noted that Sweden and Finland were more actively part of the preparation of the ESHM20 than the ESHM13.

Extending the ESHM13 and ESHM20 results beyond 5000-year return periods is not recommended, since very low-activity faults were not considered and the

ground-motion models may have been insufficiently described (Woessner et al. 2015; L. Danciu, private communication, 2023). Further investigations, such as site-specific hazard assessments, are necessary for the return periods relevant to NPPs. Danciu et al. (2024) also points out that the ground motion hazard estimates do not directly translate into design values, as these must be provided by national design codes or Nationally Determined Parameters in EN Eurocodes.

In the future, the European Facilities for Earthquake Hazard and Risk (EFEHR) will retain an important role in providing open access to state-of-the-art, reproducible data, models and information on earthquake hazard and risk analysis. How and when the ESHM20 and the European seismic risk model ESRM20 will possibly be reviewed and/or updated is currently an open question. When moving toward the next generation of hazard and risk models, the new challenges and opportunities include physics-based modeling and the use of artificial intelligence. Gerstenberger et al. (2020) advocate more science-driven models, such as replacing time-independent seismicity models by time-dependent ones. Anyway, the EFEHR will enrich and serve as an incentive for further development of national hazard models in Europe in the coming years. The second-generation EC8 (EN1998-1-1) is planned to be officially released in 2024.

We consider the following directions and recommendations for future work on seismic hazard in Fennoscandia to be important:

- Both ESHM models use a shear-wave velocity in the upper 30 meters of the crust (the so called V_{s30}) which is uniform across Europe and at 800 m/s much too slow for most of the cratonic part of Fennoscandia. V_{s30} in these regions are usually on the order of 2500–3000 m/s, which if implemented in the hazard models, would generally slightly decrease the hazard.

- As ESHM20 has a magnitude cut-off at M_w3.5, the earthquake data available in Fennoscandia are not used to their full potential. As this report shows, there is rarely enough data in Fennoscandia in ESHM20 to draw statistically stringent conclusions. Ongoing work in the Fennoscandian countries on new seismic hazard models utilizing the significantly larger data set outlined in this report should be continued and supported. This will provide regionally relevant data in the areas of Fennoscandia that have significant seismic activity, albeit of lower magnitude. Other regions of Fennoscandia have very low activity rates and those regions will remain problematic for PSHA.

- Incorporation of uncertainties in a logic-tree framework should not be a pruned version of the logic trees designed at high-seismicity regions, but be specifically tailored for low-seismicity regions.

- As new national models are being developed, it is important that the transnational collaboration continues in order to create a harmonized Fennoscandian hazard model, which is continuous across the national borders.

8. Conclusions

The European Seismic Hazard Model 2013 (ESHM13) and its successor ESHM20 were designed to utilize state-of-the art procedures homogeneously applied for the pan-European region and Türkiye, with data compilation and methods harmonized across country borders. While this harmonization certainly is valuable in order to be able to compare seismic hazard from region to region, it requires careful design in order to not impose difficult to meet constraints. For low-seismicity regions such as Fennoscandia, one such constraint is the cut-off magnitude of Mw 3.5, as applied in ESHM20, which significantly reduces the number of earthquakes available for the assessment. The lack of data causes problems for the statistical treatment of different regions and requires very large areas in order to capture enough events in the recurrence calculations.

In this report, we have compared the seismic hazard results from ESHM13 to ESHM20 for Fennoscandia with a focus on the five nuclear power plant sites in Fennoscandia; Ringhals in southwestern Sweden, Oskarshamn in southeastern Sweden, Forsmark on the central east coast of Sweden, Olkiluoto on the southwestern coast of Finland and Loviisa on the northern coast of the Gulf of Finland. We find that:

- The number of earthquakes included in the two models are almost identical, the onshore and near-shore Fennoscandian part of the catalog only increased by 8 events, from 362 in ESHM13 to 370 in ESHM20. 14 events were removed from the ESHM13 catalog while 22 events were added to the ESHM20 catalog.
- We discovered an error in the assignment of *a*- and *b*-values to area source zone SEAS409 in ESHM20, where Ringhals is located. The area uses an *a*-value of 1.65 and a *b*-value of 0.84, these should have been 2.29 and 1.04, respectively, inherited from tectonic source zone TSZ007. The recurrence parameters used decrease the return time of larger earthquake in comparison to the correct values, thereby increasing the hazard somewhat.
- As the earthquake data and the earthquake source zones are very similar between the two models, differences between the results of ESHM13 and ESHM20 depend mostly on a complete update of ground motion models, a significantly expanded logic tree and improved methodologies and algorithms.
- From ESHM13 to ESHM20 seismic hazard in terms of peak-ground acceleration (PGA) has increased at Olkiluoto, Forsmark and Oskarshamn and for return periods longer than 2500 years at Loviisa. It has decreased in Ringhals and for short return periods at Loviisa. The hazard in terms of mean PGA for an annual exceedance probability of $2 \cdot 10^{-4}$, or 5000-year return period, varies from 0.028 g at Loviisa to 0.0744 g at Oskarshamn in ESHM20. For ESHM13, that span was from 0.016 g at Olkiluoto to 0.1211 g at Ringhals.

- The standard deviations of the hazard distributions have increased significantly from ESHM13 to ESHM20, from 50% increase at Ringhals to a 15-fold increase at Forsmark. The large increase in standard deviation implies that the coefficient of variation, the ratio of the standard deviation to the mean, a measure of the dispersion of the probability distribution, has also increased significantly from ESHM13 to ESHM20. This increase in uncertainty depends to a large extent on the inclusion of a larger logic tree in the hazard calculation, better accounting for epistemic uncertainty. However, uncertainty ranges as wide as in the case of Loviisa may make the evaluation of the hazard difficult.
- We applied four different tests of how robust, or significant, the differences between the two hazard models are: (i) the change in the mean annual frequency of exceedance (AFE) for a particular ground motion level (McGuire 2012), (ii) the size of the ratio of the difference in mean hazard to the RMS of the standard deviations (Malhota 2014, 2015), (iii) if the mean ground motion of the AFE of interest in ESHM13 is outside the 25^{th} – 75^{th} fractiles of ESHM20 (Abrahamson 2017) and (iv) the size of the logarithm of the ratio of mean ground motions at the AFE of interest minus half the standard deviation (Abrahamson 2017). Test (i) showed significant differences between the means in ESHM13 and ESHM20 at small AFE (10^{-4} and 10^{-6}, outside the scope of the ESHMs). Test (ii) did not show a large difference between the two models for any return period or NNPs, except for AFE 10^{-6} at Forsmark and Oskarshamn. This is mostly due to the large increase in standard deviations. Tests (iii) and (iv) showed mostly contradictory results, one or the other indicating robust differences, for all return periods and NPPs, except for at Oskarshamn where the two tests agreed that the models are robustly different for all AFEs. We find the tests inconclusive, although one of the tests always indicate that the models are different, at all return periods and NPPs.
- The ESHMs are not intended as site-specific hazard models and are not applicable to annual probabilities of exceedance below $2{\cdot}10^{-4}$, or return periods beyond 5000 years. Site-specific models are necessary for nuclear power plants.
- There is significantly more earthquake data available in Fennoscandia than was used in ESHM20. By lowering the magnitude threshold, more of the area source zones can have individual recurrence parameters calculated based on statistically significant data sets and spatial variations in seismicity can be better accounted for. For the very smallest magnitude earthquakes more research is warranted in order to assess the validity of the extrapolation to large earthquakes in hazard analysis.
- The collaboration between seismological institutes in Sweden, Finland, Norway and Denmark is good and has been increasing since the 2010s.

9. References

Abrahamson N (2017) Treatment of epistemic uncertainty in PSHA results. PSHA workshop, Lenzburg, Switzerland

Akkar S, Bommer JJ (2010) Empirical equations for the prediction of PGA, PGV, and spectral accelerations in Europe, the Mediterranean Region, and the Middle East. Seismol Res Lett 81:195–206. https://doi.org/10.1785/gssrl.81.2.195

Bommer JJ, Scherbaum F (2008) The use and misuse of logic trees in probabilistic seismic hazard analysis. Earthquake Spectra 24:997–1009. https://doi.org/10.1193/1.2977755

Bommer JJ, Scherbaum F, Bungum H, Cotton F, Sabetta F, Abrahamson NA (2005) On the use of logic trees for ground-motion prediction equations in seismic-hazard analysis. Bull Seismol Soc Am 95:377–389. https://doi.org/10.1785/0120040073

Budnitz RJ, Apostolakis G, Boore DM, Cluff LS, Coppersmith KJ, Cornell CA, Morris PA (1997) Recommendations for Probabilistic Seismic Hazard Analysis: Guidance on uncertainty and use of experts. NUREG/CR-6372 UCRL- ID – 122160, vol. 1

Campbell KW (2003) Prediction of strong ground motion using the hybrid empirical method and its use in the development of ground-motion (attenuation) relations in eastern North America. Bull Seismol Soc Am 93:1012–1033. https://doi.org/10.1785/0120020002

Cauzzi C, Faccioli E (2008) Broadband (0.05 to 20 s) prediction of displacement response spectra based on worldwide digital records. J Seismol 12:453–475. https://doi.org/10.1007/s10950-008-9098-y

CEN (2004) Eurocode 8, design of structures for earthquake resistance—part 1: general rules, seismic actions and rules for buildings. Comité europeén de normalisation, Brussels

Chiou BSJ, Youngs RR (2008) An NGA model for the average horizontal component of peak ground motion and response spectra. Earthq Spectra 24:173–215. https://doi.org/10.1193/1.2894832

Cohen J (1977) Statistical Power Analysis for the Behavioral Sciences. Academic Press, ISBN: 978-0-12-179060-8. https://doi.org/10.1016/C2013-0-10517-X

Coppersmith KJ, Salomone LA, Fuller CW et al (2012) Technical report: central and eastern United States seismic source characterization for nuclear facilities, chapter 5. Palo Alto, CA, USA

Cornell CA (1968) Engineering seismic risk analysis. Bull Seismol Soc Am 58:1583–1606. Erratum 59:1733

Crowley H, Dabbeek J, Despotaki V, Rodrigues D, Martins L, Silva V, Romão X, Pereira N, Weatherill G, Danciu L (2021) European Seismic Risk Model (ESRM20).

EFEHR Technical Report 002 V1.0.0. https://doi.org/10.7414/EUC-EFEHR-TR002-ESRM20

Danciu L, Şeşetyan K, Demircioglu M, Gülen L, Zare M, Basili R et al. (2018) The 2014 Earthquake Model of the Middle East: Seismogenic sources. Bull Earthquake Eng 16:3465–3496. https://doi.org/10.1007/s10518-017-0096-8

Danciu L, Nandan S, Reyes C, Basili R, Weatherill G, Beauval C, Rovida A, Vilanova S, Sesetyan K, Bard P-Y, Cotton F, Wiemer S, Giardini D (2021) The 2020 update of the European Seismic Hazard Model: Model Overview. EFEHR Technical Report 001, v1.0.0. https://doi.org/10.12686/a15

Danciu L, Giardini D, Weatherill G, Basili R, Nandan S, Rovida A, Beauval C, Bard P-Y, Pagani M, Reyes CG, Sesetyan K, Vilanova S, Cotton F, Wiemer S (2024) The 2020 European Seismic Hazard Model: Overview and Results. EGUsphere [preprint]. https://doi.org/10.5194/egusphere-2023-3062

Delavaud E, Cotton F, Akkar S, Scherbaum F, Danciu L, Beauval C, Drouet S, Douglas J, Basili R, Addullah Sandikkaya M, Segou M, Facciolo E, Theodoulidis N (2012) Toward a ground-motion logic tree for probabilistic seismic hazard assessment in Europe. J Seismol 16:451–473.
https://doi.org/10.1007/s10950-012-9281-z

Douglas J (2018) Calibrating the backbone approach for the development of earthquake ground motion models. In: Best practice in physics-based fault rupture models for seismic hazard assessment of nuclear installations: issues and challenges towards full seismic risk analysis, 2018-05-14–2018-05-16, CEA – Cadarache–Château. https://strathprints.strath.ac.uk/63991

Douglas J, Ulrich T, Bertil D, Rey J (2014) Comparison of the ranges of uncertainty captured in different seismic-hazard studies. Seismol Res Lett 85:977–985. https://doi.org/10.1785/0220140084

Douglas J, Crowley H, Silva V, Marzocchi W, Danciu L, Pinho R (2023) Methods for evaluating the significance and importance of differences amongst probabilistic seismic hazard results for engineering and risk analyses: A review and insights. EGUsphere [preprint]. https://doi.org/10.5194/egusphere-2023-991
https://doi.org/10.12686/a15

Esteva L (1969) Seismicity prediction: A Bayesian approach. Proc. World Conf. Earthquake Engineering, 4th, Santiago, Chile, 1:172–184

Fülöp L, Jussila V, Aapasuo R, Vuorinen T, Mäntyniemi P (2020) A ground-motion prediction equation for Fennoscandian nuclear installations. Bull Seismol Soc Am 110:1211–1230. https://doi.org/10.1785/0120190230

Fülöp L, Mäntyniemi P, Malm M, Toro G, Crespo MJ, Schmitt T, Burck S, Välikangas P (2023) Probabilistic seismic hazard analysis in low-seismicity regions: An investigation of sensitivity with a focus on Finland. Nat Hazards 116:111–132. https://doi.org/10.1007/s11069-022-05666-4

GEM (2022) The OpenQuake-engine User Manual. Global Earthquake Model (GEM) OpenQuake Manual for Engine version 3.18.0. https://doi.org/10.13117/GEM.OPENQUAKE.MAN.ENGINE. 3.18.0

Gerstenberger MC, Marzocchi W, Allen T, Pagani M, Adams J, Danciu L et al. (2020) Probabilistic seismic hazard analysis at regional and national scales: State of the art and future challenges. Rev Geophys 58:e2019RG000653. https://doi.org/10.1029/2019RG000653

Giardini D, Basham P (1993) The Global Seismic Hazard Assessment Program (GSHAP). Ann Geofis 36:3–13. https://doi.org/10.4401/ag-4256

Goulet CA, Bozorgnia Y, Abrahamson N, Kuehn N, Al Atik L, Youngs R, Graves R, Atkinson G (2018) Central and Eastern North America Ground-Motion Characterization NGA-East. Final Report (No. PEER 2018/08). Pacific Earthquake Engineering Research Center, California, Berkeley

Grünthal G, Wahlström R (2012) The European-Mediterranean Earthquake Catalogue (EMEC) for the last millennium. J Seismol 16:535–570. https://doi.org/10.1007/s10950-012-9302-y

Hanks TC, Abrahamson NA, Boore DM, Coppersmith KJ, Knepprath NE (2009) Implementation of the SSHAC Guidelines for Level 3 and 4 PSHAs – Experience gained from actual applications. Open-File Report 2009-1093, U.S. Geological Survey, Reston, Va.

Hiemer S, Woessner J, Basili R, Danciu L, Giardini D, Wiemer S (2014) A smoothed stochastic earthquake rate model considering seismicity and fault moment release for Europe. Geophys J Int 198:1159–1172. https://doi.org/10.1093/gji/ggu186

IAEA (2016) Diffuse seismicity in seismic hazard assessment for site evaluation of nuclear installations. Safety Reports Series No. 89, International Atomic Energy Agency, Vienna, Austria

Jiménez MJ, Giardini D, Grünthal G and SESAME Working Group (Erdik M, García-Fernández M, Lapajne J, Makropoulos K, Musson R, Papaioannou Ch, Rebez A, Riad S, Sellami S, Shapira A, Slejko D, van Eck T, El Sayed A) (2001) Unified seismic hazard modelling throughout the Mediterranean region. Boll Geofis Teor Appl 42:3–18

Johnston AC, Coppersmith KJ, Kanter LR, Cornell CA (1994) The earthquakes of stable continental regions. Vol. 1: Assessment of large earthquake potential. EPRI Report TR-102261-V1, Schneider JF (ed), Palo Alto, CA: Electric Power Research Institute, 370 pp.

Joshi N, Lund B, Roberts R (2023) Probabilistic seismic hazard assessment of Sweden, Nat Hazards Earth Syst Sci Discuss. [preprint], https://doi.org/10.5194/nhess-2023-213, in review.

Jussila V, Fälth B, Mäntyniemi P, Voss P, Lund B, Fülöp L (2021) Application of a hybrid modeling method for generating synthetic ground motions in Fennoscandia, Northern Europe. Bull Seismol Soc Am 111:507–2526. https://doi.org/10.1785/0120210081

Kagan YY, Jackson DD (2000) Probabilistic forecasting of earthquakes. Geophys J Int 143:438–453. https://doi.org/10.1046/j.1365-246X.2000.01267.x

Kotha SR, Weatherill G, Bindi D, Cotton F (2020) A regionally-adaptable ground-motion model for shallow crustal earthquakes in Europe. Bull Earthquake Eng 18:4091–4125. https://doi.org/10.1007/s10518-020-00869-1

Kozlovskaya E, Narkilahti J, Nevalainen J, Hurskainen R, Silvennoinen H (2016) Seismic observations at the Sodankylä Geophysical Observatory: History, present, and the future. Geosci Instrum Method Data Syst 5:365-382

Kulkarni RB, Youngs RR, Coppersmith KJ (1984) Assessment of confidence intervals for results of seismic hazard analysis. In: Proceedings, Eighth World Conference on Earthquake Engineering, vol. 1, San Francisco, pp. 263–270

Lanzano G, Sgobba S, Luzi L, Puglia R, Pacor F, Felicetta C, D'Amico M, Cotton F, Bindi D (2019) The pan-European Engineering Strong Motion (ESM) Flatfile: compilation criteria and data statistics. Bull Earthquake Eng 17:561–582.
https://doi.org/10.1007/s10518-018-0480-z

Malhotra PK (2014) Cost of uncertainty in seismic hazard. Technical report, StrongMotions Inc., Sharon, USA

Malhotra PK (2015) Myth of probabilistic seismic hazard analysis. Structure, July, 58–59

Mäntyniemi P, Malm M, Burck S, Okko O, Välikangas P, Fülöp L (2021) Sensitivity of seismic hazard analysis in Finland: Overview of the SENSEI project. ATS Ydintekniikka 50:19–23

Mäntyniemi P, Malm M, Rinne L, Fülöp L (2023) Valorization of probabilistic seismic hazard results in Finland. Research report VTT-R-00978-22, VTT Technical Research Centre of Finland, 41 p. http://hdl.handle.net/10138/567972

McGuire RK (1993) Computations of seismic hazard. Ann Geofis 36:181–200. https://doi.org/10.4401/ag-4263

McGuire RK (1995) Probabilistic seismic hazard analysis and design earthquakes: Closing the loop. Bull Seismol Soc Am 85:1275–1284.

McGuire RK (2008) Probabilistic seismic hazard analysis: Early history. Earthq Eng Struct Dyn 37:329–338. https://doi.org/10.1002/eqe.765

McGuire RK (2012) Precision of Seismic Hazard Evaluations in Central and Eastern North America. Proceedings of the 15th World Conference on Earthquake Engineering, Paper number 5501

Olsen, O, Olsen, L, Gibbons, SJ, Ruud, BO, Høgaas, F, Johansen, TA, Kværna, T (2021) Postglacial Faulting in Norway: Large Magnitude Earthquakes of the Late Holocene Age. In: Glacially-Triggered Faulting, edited by Steffen H, Olesen O, Sutinen R, p. 198–217, Cambridge University Press. https://doi.org/10.1017/9781108779906.015

Ottemöller L, Michalek J, Christensen J-M, Baadshaug U, Halpaap F, Natvik Ø, Kværna T, Oye V (2021) UiB-NORSAR EIDA Node: Integration of seismological data in Norway. Seismol Res Lett 92:1491–1500. https://doi.org/10.1785/0220200369

Pagani M, Monelli D, Weatherill G, Danciu L, Crowley H, Silva V, Henshaw P, Butler L, Nastasi M, Panzeri L, Simionato M, Vigano D (2014) OpenQuake engine: An open hazard (and risk) software for the Global Earthquake Model. Seismol Res Lett 85:692–702. https://doi.org/10.1785/0220130087

Rovida A, Antonucci A (2021) EPICA – European PreInstrumental earthquake Catalogue, version 1.1. https://doi.org/10.13127/EPICA.1.1

Soosalu H, Uski M, Komminaho K, Veski A (2022) Recent intraplate seismicity in Estonia, East European Platform. Seismol Res Lett 93:1800–1811. https://doi.org/10.1785/0220210277

Solomos G, Pinto Vieira A, Dimova S (2008) A Review of the Seismic Hazard Zonation in National Building Codes in the Context of Eurocode 8. EUR 23563 EN. Luxembourg (Luxembourg): OPOCE, JRC48352

Toro, G.R. (2002) Modification of the Toro et al. (1997) attenuation equations for large magnitudes and short distances, unpublished report, Risk Engineering Inc., June 12.

USNRC (2012) Practical implementation guidelines for SSHAC level 3 and 4 hazard studies. U.S. Nuclear Regulatory Commission, NUREG-2117, Revision 1

Veikkolainen T, Kortström J, Vuorinen T, Salmenperä I, Luhta T, Mäntyniemi P, Hillers G, Tiira T (2021) The Finnish national seismic network: towards fully automated analysis of low-magnitude seismic events. Seismol Res Lett 92:1581–1591. https://doi.org/10.1785/0220200352

Voss, P, Dahl-Jensen, T, Larsen, TB (2015) Earthquake Hazard in Denmark. GEUS. Danmarks og Grønlands Geologiske Undersøgelse Rapport Vol. 2015 No. 24 https://doi.org/10.22008/gpub/30674

Weatherill G, Cotton F (2020) A ground motion logic tree for seismic hazard analysis in the stable cratonic region of Europe: regionalization, model selection and development of a scaled backbone approach. Bull Earthquake Eng 18:6119–6148. https://doi.org/10.1007/s10518-020-00940-x

Weatherill G, Kotha SR, Cotton F (2020) A regionally-adaptable "scaled backbone" ground motion logic tree for shallow seismicity in Europe: Application to the 2020 European seismic hazard model. Bull Earthquake Eng 18:5087–5117. https://doi.org/10.1007/s10518-020-00899-9

Weatherill G, Kotha SR, Danciu L, Vilanova S, Cotton, F (2023a) Modelling seismic ground motion and its uncertainty in different tectonic contexts: Challenges and application to the 2020 European Seismic Hazard Model (ESHM20). Nat Hazards Earth Syst Sci, Discuss. [preprint], https://doi.org/10.5194/nhess-2023-124, in review

Weatherill G, Cotton F, Daniel G, Zentner I, Iturrieta P, Bosse C (2023b) Strategies for comparison of modern probabilistic seismic hazard models and insights from

the Germany and France border region. Nat Hazards Earth Syst Sci, Discuss. [preprint], https://doi.org/10.5194/nhess-2023-98, in review

Weichert DH (1980) Estimation of the earthquake recurrence parameters for unequal observation periods. Bull Seismol Soc Am 70:1337–1346

Wheeler RL (2009) Methods of Mmax estimation east of the Rocky Mountains. Open file report 2009-1018, USGS.

Wheeler RL (2011) Reassessment of stable continental regions of Southeast Asia. Seismol Res Lett 82:971-983. https://doi.org/10.1785/gssrl.82.6.971

Woessner J, Laurentiu D, Giardini D, Crowley H, Cotton F, Grünthal G, Valensise G, Arvidsson R, Basili R, Demircioglu MB, Hiemer S, Meletti C, Musson RW, Rovida AN, Sesetyan K, Stucchi M, The SHARE Consortium (2015) The 2013 European Seismic Hazard Model: key components and results. Bull Earthquake Eng 13:3553–3596. https://doi.org/10.1007/s10518-015-9795-1

Youngs RR, Goulet CA, Bozorgnia Y, Kuehn N, Al Atik L, Graves RW, Atkinson GM (2021) NGA-East ground-motion characterization model Part II: Implementation and hazard implications. Earthquake Spectra 37(S1):1283–1330.
https://doi.org/10.1177/87552930211007503

COMPARING EUROPEAN SEISMIC HAZARD MODELS

The European Seismic Hazard Model 2020 (ESHM20) succeeds the 2013 model (ESHM13) using the same approach of state-of-the art procedures homogeneously applied to the entire pan-European region, without country-border issues. The models are not intended as sitespecific hazard models, they are not applicable to annual probabilities of exceedance below 2·10-4 and do not replace national hazard models. For Fennoscandia, the update only increases the earthquake data set by eight events, but the seismic source zones were updated, there was a complete change of ground motions models and the logic tree was significantly expanded.

The mean hazard, in terms of peak-ground-acceleration (PGA), has increased from ESHM13 to ESHM20 at the nuclear power plants (NPPs) in Loviisa, Olkiluoto, Forsmark and Oskarshamn, a change of the same order of magnitude as the means in ESHM13. At Ringhals the mean hazard has decreased by more than 50%, and would likely have been even lower had there not been a mistake in parameter settings in ESHM20 for the Ringhals source area. In addition, the standard deviations of the PGA distributions have increased considerably at all locations except at Ringhals, where the increase is more modest. In order to assess the significance of the differences, we applied four different tests to the models, addressing different aspects of the model results. The test results were inconclusive in that some tests indicated robust differences while others did not.

ESHM20 only uses earthquakes with magnitude 3.5 or higher, which severely limits the amount of data from Fennoscandia. The modern seismic networks in Fennoscandia record thousands of smaller earthquakes every year which could be included in hazard assessments, thereby significantly improving the models.

A new step in energy research

The research company Energiforsk initiates, coordinates, and conducts energy research and analyses, as well as communicates knowledge in favor of a robust and sustainable energy system. We are a politically neutral limited company that reinvests our profit in more research. Our owners are industry organisations Swedenergy and the Swedish Gas Association, the Swedish TSO Svenska kraftnät, and the gas and energy company Nordion Energi.

Energiforsk